iScience

Article

Swi4-dependent SWI4 transcription couples cell size to cell cycle commitment

Graphical abstract

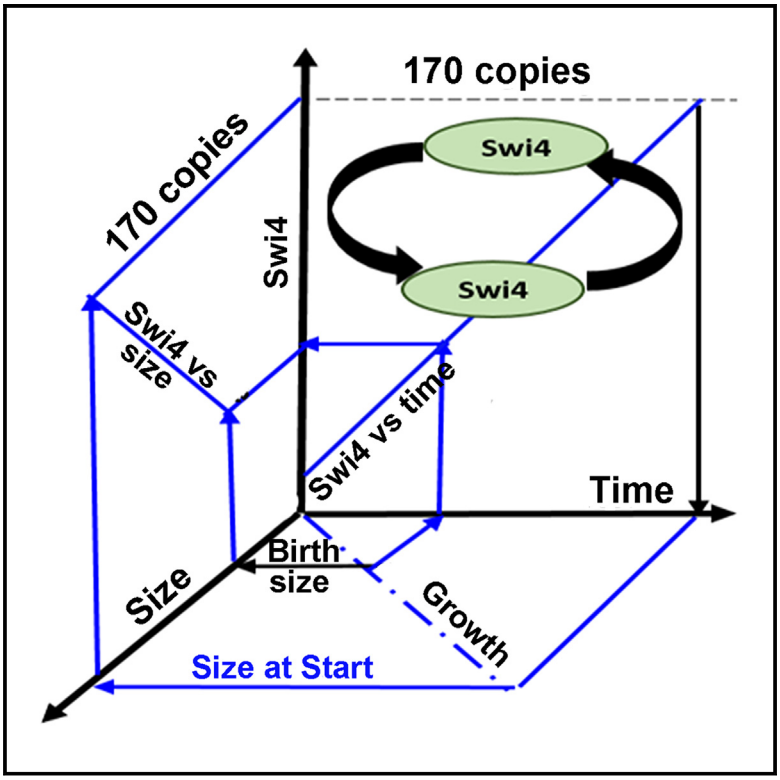

Highlights

- Swi4 protein activates *SWI4* transcription in a Swi4 binding site dependent manner
- Ectopic expression of Swi4 induces *SWI4* expression and accelerates the G1/S transition
- Quantitative microscopy suggests a copy-number threshold Swi4 is required for Start
- A Swi4 threshold predicts cell size in different genetic and nutritional contexts

Authors

Pooja Goswami, Abhishek Ghimire, Carleton Coffin, ..., Mike Tyers, Sylvain Tollis, Catherine A. Royer

Correspondence

quantcellbiolconsulting@gmail.com (M.T.), sylvain.tollis.umontreal@gmail.com (S.T.), royerc@rpi.edu (C.A.R.)

In brief

Molecular biology; Cell biology

Goswami et al., 2025, iScience *28*, 112027
March 21, 2025
https://doi.org/10.1016/j.isci.2025.112027

CellPress

iScience

CellPress
OPEN ACCESS

Article

Swi4-dependent SWI4 transcription couples cell size to cell cycle commitment

Pooja Goswami,[1,6,10] Abhishek Ghimire,[1,10] Carleton Coffin,[1] Jing Cheng,[2] Jasmin Coulombe-Huntington,[3,7] Ghada Ghazal,[3] Yogitha Thattikota,[2,8] María Florencia Guerra,[4] Mike Tyers,[2,*] Sylvain Tollis,[3,4,9,*] and Catherine A. Royer[1,4,5,11,*]

[1]Department of Biological Sciences, Rensselaer Polytechnic Institute, Troy, NY 12180, USA
[2]Program in Molecular Medicine, Peter Gilgan Centre for Research and Learning, The Hospital for Sick Children, Toronto, ON M5G 0A4, Canada
[3]Institute of Research in Immunology and Cancer, University of Montreal, Montreal, QC H3T1J4, Canada
[4]Department of Environmental and Biological Sciences, Faculty of Science, Forestry and Technology, University of Eastern Finland, 70210 Kuopio, Finland
[5]Centre de Biochimie Structurale INSERM U1054, University of University of Montpellier, 34090 Montpellier, France
[6]Present address: Department of Neurology, Brain Science Institute, Johns Hopkins University School of Medicine, Baltimore, MD 21205, USA
[7]Present address: Department of Bioengineering, McGill University, Montreal, QC H3A 0E9, Canada
[8]Present address: Montreal Neurological Institute, McGill University, Montréal, QC H3A 2B4, Canada
[9]Present address: Institute of Biomedicine, School of Medicine, Faculty of Health Sciences, University of Eastern Finland, Joensuu, 70211 Kuopio, Finland
[10]These authors contributed equally
[11]Lead contact
*Correspondence: quantcellbiolconsulting@gmail.com (M.T.), sylvain.tollis.umontreal@gmail.com (S.T.), royerc@rpi.edu (C.A.R.)
https://doi.org/10.1016/j.isci.2025.112027

SUMMARY

Growth-dependent accumulation of the G1/S transcription factor SBF, composed of Swi4 and Swi6, occurs in G1 phase in budding yeast and is limiting for commitment to division, termed Start. Here, we investigate the mechanisms for the size dependence of Swi4 accumulation using different genetic contexts and quantitative scanning number and brightness microscopy. Mutation of SBF binding sites in the *SWI4* promoter or disruption of SBF activation resulted in ~33–50% decrease in Swi4 accumulation rate and concordantly increased cell size at Start. Ectopic inducible expression of Swi4 in G1 phase cells increased production of Swi4 from the endogenous promoter, upregulated transcription of the G1/S regulon, and accelerated Start. A threshold model in which Swi4 titrates SBF binding sites in G1/S promoters predicted the effects of nutrients, ploidy, and G1/S regulatory mutations on cell size. These results exemplify how transcription factor auto-production can refine a cell state transition.

INTRODUCTION

The G1/S transition of the cell cycle is controlled at the transcriptional level in organisms from yeast to humans.[1,2] In budding yeast, this transition (termed Start) is activated by the SCB Binding Factor (SBF) and the MIu1-box binding factor (MBF) transcription factor (TF) complexes,[3] which govern expression of ~200 genes in the G1/S regulon (see simplified schematic, Figure 1). These complexes comprise the same Swi6 activator subunit, and distinct DNA-binding subunits, Swi4 and Mbp1, respectively. SBF and MBF bind to target sites, Swi4/6 cell cycle box (SCB) and MIu1 cell cycle box (MCB), present in promoters of the G1/S regulon.[3–5] The timing of the G1/S transition relative to cell growth determines cell size at Start. While deletion of *MBP1* in cells grown on rich nutrients does not significantly increase cell size, *swi4Δ* mutants are extremely large, demonstrating that under these conditions, SBF is the dominant transcriptional activator of Start.[6–8] Indeed, *SWI4* gene dosage was shown previously to be important for balanced cell growth and division[9] and appeared to be rate limiting for the G1/S transition.[10] Transcriptional activation by SBF is repressed during G1 phase by Whi5, which binds to and inactivates SBF.[11] The SBF-Whi5 complex is phosphorylated on multiple sites by the Cln-Cdc28 cyclin-dependent kinases in late G1, resulting in Whi5 dissociation and export from the nucleus, which is the earliest molecular indicator of Start.[12,13] A triple *CLN1/2/3* deletion or inactivation of Cdc28 causes permanent arrest at Start.[14–16] Deletion of the upstream G1 cyclin gene *CLN3* markedly delays SBF activation and increases cell size at Start.[16] Translation of the *CLN3* mRNA may couple the protein synthesis rate to Start activation.[17] Importantly, the downstream *CLN1/2* genes are part of the G1/S regulon and form a phosphorylation-driven positive feedback loop that activates SBF.[18] Deletion of *WHI5* causes a small cell size phenotype that is epistatic to the large

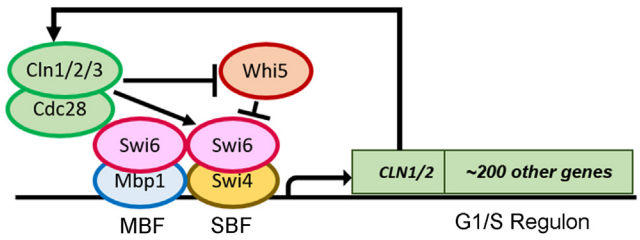

Figure 1. A simplified schematic of the network of factors implicated in Start

sized caused by deletion of *SWI4*,[11] underscoring the central role of SBF at Start.

We previously found that the total copy numbers of Swi4 and Mbp1, as calculated from absolute concentrations and cell size, are limiting with respect to their ~200 target G1/S promoters in early G1 phase.[19] We also found that Swi4 absolute nuclear concentration scales positively with growth, increasing 1.6- to 2-fold in G1 phase, while the concentrations of Mbp1 and Swi6, like that of Whi5, remain constant.[19] In small cells, Swi4 copy number is much lower than that of Mbp1, Swi6, or Whi5, but the positive scaling of Swi4 with growth in G1 phase leads to a ~5- to 6-fold increase in Swi4 copy number prior to Start. The copy numbers of the other SBF/MBF subunits also increase during G1 phase, leading to a titration model for Start whereby SBF/MBF increase throughout G1 phase until they reach abundance that sufficiently saturates G1/S promoters and activates the G1/S regulon. While these prior results are in contradiction with other less quantitative work,[20,21] further time-dependent control experiments[22] have validated our initial conclusions, demonstrating that scanning number and brightness (sN&B) imaging provides accurate quantitative information about the absolute concentration and copy number of G1/S TFs in budding yeast cells. Thus, while Cln-Cdc28 dependent phosphorylation and nuclear export of Whi5 are clearly key determinants of the Start transition, subsaturating SBF copy number in small cells and growth-dependent SBF accumulation may help to gate Start.[19,23] One prediction of this promoter titration model is that Start should be activated by a similar copy number of SBF/MBF irrespective of genetic background or growth conditions.

SBF is the major activator of G1/S transcription in rich nutrients,[11] and Swi4 is cyclically expressed.[9] The low levels of Swi4 in newborn cells and its positive differential accumulation with respect to growth and to the other G1/S TFs[19] raises the key question of how the expression of *SWI4* during G1 phase is controlled. An upstream activating sequence (UAS) in the *SWI4* promoter contains several SCB/MCB sites, as well as an early cell cycle box (ECB) site.[24] The Mcm1 transcriptional activator, which binds the ECB,[10] contributes to *SWI4*, *SWI6*, and *MBP1* expression in M/G1.[10,25,26] Deletion of 140 base pairs corresponding to this entire UAS was shown to cause a 10-fold decrease in Swi4 levels.[24] Deletion of *SWI6* also decreased Swi4 levels and abrogated *SWI4* cyclic expression,[24] while ectopic expression of *CLN3* induced expression of *SWI4*,[16] suggesting that Swi4 may contribute to its own expression. Furthermore, genome-wide Chromatin ImmunoPrecipitation sequencing (CHIP-seq) experiments demonstrated a physical interaction of Swi4 with its own promoter.[4,25] Based on these observations, Swi4-dependent *SWI4* expression has been postulated.[4,24,25,27] However, this mechanism has never been quantitatively established, nor its potential role at Start evaluated. Moreover, it is not firmly established whether MBF contributes to *SWI4* expression, although *SWI4* mRNA levels decrease relative to WT cells in an *mbp1Δ* strain,[27] and Mbp1 binds to the *SWI4* promoter in ChIP-seq experiments.[4,25]

In the present work, we sought to define and quantify the molecular mechanisms underlying *SWI4* expression and to test the G1/S TF titration hypothesis for Start. We quantitatively determined the effects of Swi4, other G1/S regulatory proteins, and transcriptional regulatory elements within the *SWI4* promoter on Swi4 production. Using the sN&B particle counting technique,[19] we found that deletion or mutation of different combinations of the SCB/MCB sites in the *SWI4* promoter resulted in a 33–46% decrease in the rate of accumulation of Swi4 copy number with respect to growth. Disruption of phosphorylation of the SBF-Whi5 complex, resulted in a ~50% decrease in Swi4 accumulation rate, further implicating SBF in its own production. Deletion of *MBP1* decreased Swi4 protein production only slightly. Ectopic expression of Swi4 from a β-estradiol (BE2)-dependent promoter led to a BE2-dependent increase of endogenous Swi4 production, which was accompanied by upregulation of genes in the G1/S regulon. A similar threshold of Swi4 copy number at Start was observed under different genetic contexts, supporting the hypothesis that titration of the G1/S promoters gates Start. Together, these results demonstrate that SBF-mediated *SWI4* autoregulation contributes to the timing of the G1/S transition.

RESULTS

sN&B yields absolute protein concentrations and copy numbers

We have previously used the sN&B technique to quantify G1/S TF concentration and copy number as a function of cell size.[19] This technique, which provides absolute values of protein concentration, causes negligible photobleaching (≤5%) due to very rapid raster scanning, and with 2-photon excitation, minimal contributions of background autofluorescence. In our implementation of sN&B, we rely not on the fluctuations in fluorescence directly but on a calibration factor, the molecular brightness of GFP itself, determined separately for millions of pixels in hundreds of cells expressing free GFP (Methods S1, Figure S1).[19] This calibration-based approach extends the accessible range of protein measurements to very low concentrations by averaging the intensity over all relevant pixels to limit noise, and to very high concentrations where fluctuations tend toward zero. This approach also renders the determined values much less susceptible to uncertainty in fluorescence detection.

Swi4 binding sites in the *SWI4* promoter contribute to Swi4 protein expression

Using this sN&B approach, we measured the absolute nuclear concentration of Swi4 fused to fast folding-monomeric GFPmut3 (hereafter referred to as Swi4-GFP for brevity) expressed from its

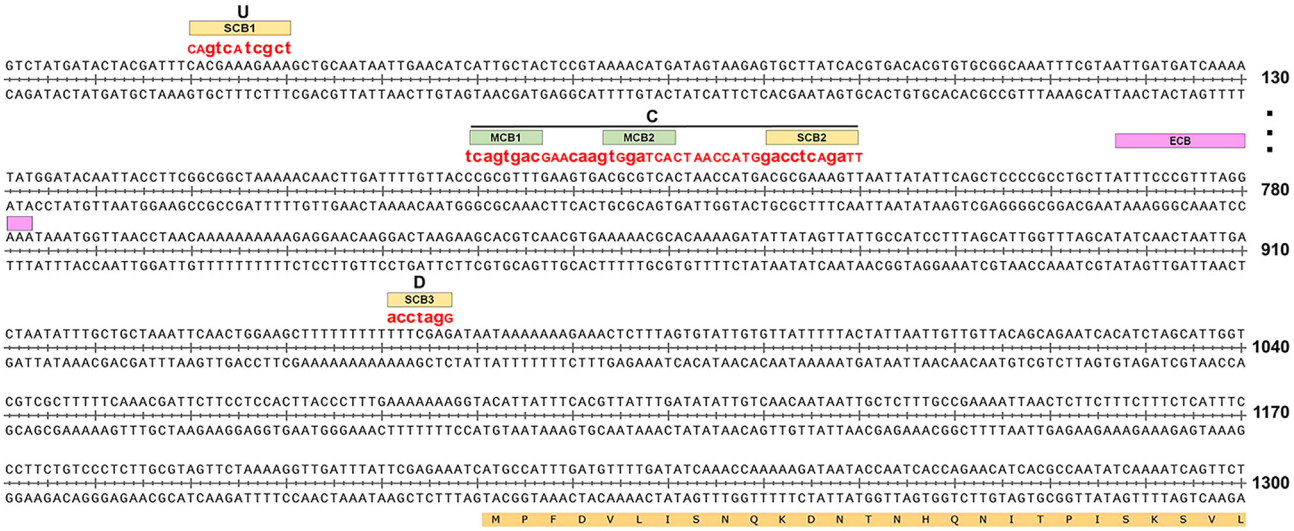

Figure 2. Mutations of the SCB/MCB sites in the SWI4 promoter

Region of the *SWI4* promoter containing the SCB/MCB sites deleted or mutated in this study. Green rectangles designate MCB sites, orange rectangles designate SCB sites, pink rectangle designates the ECB site which was not deleted in our strains. U refers to the upstream SCB1 site, C to the central site containing MCB1, MCB2 and SCB2. D refers to the downstream SCB3 site. The beginning of the *SWI4* open reading frame (ORF) is also shown in yellow with the one letter amino acid abbreviations. WT and mutated sequences are listed in Table S1. The red sequences below each site correspond to the mutated sequences used in this study.

endogenous locus in single cells asynchronously growing in SC+2% glucose medium.[19] Individual cell sizes were determined from the single-cell images, and for simplicity, the nuclear volume was assumed to be ~1/7th of the total cell volume,[28] although we note that the scaling of nuclear volume with size in G1 is actually slightly sub-linear.[22] Swi4 nuclear copy number was calculated as the product of the average nuclear concentration and the estimated nuclear volume. Since Swi4 exits the nucleus sometime after budding but before mitosis,[19] the measured cells with nuclear Swi4 were predominantly either in G1 or S-phase.

We compared Swi4 protein copy numbers as a function of cell size in asynchronous populations of *SWI4-GFP* cells under control of the wild-type *SWI4* promoter versus *SWI4-GFP* strains bearing various deletions or mutations in the *SWI4* promoter region (Figures 2 and S2; Table S1). In addition to three clustered central SCB/MCB promoter sites (termed site C for central in Figure 2) situated ~30 bp upstream of the ECB site documented previously,[24] we identified two other putative SCB sites, one situated ~1,200 bp (termed site U for upstream) and the other ~270 bp upstream of the *SWI4* ORF (termed site D for downstream, position 950 in Figure 2) that could potentially contribute to *SWI4* expression.

Deletion of the central region harboring two MCB sites and one SCB site (a total of 39 bp deleted, termed Cdel, *SWI4pr$_{Cdel}$-SWI4-GFP*) decreased the rate of accumulation of Swi4-GFP protein copy number with respect to cell size (dSwi4/dsize) by 33% compared to WT. Mutation of the same central sites to non-consensus SCB/MCB sequences (Cmut, *SWI4pr$_{Cmut}$-SWI4-GFP*) resulted in a similar (37%) decrease (Figure 3A; Table 1; Table S1). This same mutation of the central promoter region, together with mutation of the downstream SCB site (C + Dmut, *SWI4pr$_{C+Dmut}$-SWI4-GFP*) also decreased Swi4-GFP accumulation (~38%), while additional mutation of the upstream SCB site (C + D + Umut, *SWI4pr$_{C+D+Umut}$-SWI4-GFP*) decreased Swi4 accumulation even further (46%) (Figure 3B; Table 1). These results establish that the MCB/SCB sites in the *SWI4* promoter are responsible collectively for about half of total Swi4 protein expression in G1/S phase haploid cells. Interestingly, in heterozygous *SWI4/SWI4-GFP* diploid cells (*i.e.*, WT promoter for both alleles but only one allele labeled with GFP), the rate of accumulation of labeled Swi4 nuclear copy number with respect to size was 58% lower than in haploids, while the deletion of the central promoter on the allele expressing Swi4-GFP lowered the accumulation rate even further (67%, Table 1; Figure S3). The total Swi4 accumulation rate with respect to size in heterozygous *SWI4/SWI4-GFP* diploids corresponded to only a 16% increase compared to haploids, even though there were two *SWI4* loci and twice as many G1/S TF target sites in diploids.

In agreement with our previously published model, in which Swi4 protein copy number is a limiting factor for cell cycle commitment,[19] deletions or mutations of the various MCB/SCB sites in the *SWI4* promoter in haploid cells led to a modest large size phenotype, as assessed by Coulter counter measurements (Figures S4A–S4C; Table S2). The average size, as derived from the sN&B images of single cells exhibiting nuclear Swi4-GFP, hence in G1/S phase, was also larger for the promoter mutants compared to WT cells (Figure S5; Table 2). This phenotype was reduced in *SWI4/SWI4-GFP* heterozygous diploids, where the mean size for the heterozygous diploid in which one allele carried the *SWI4pr$_{Cdel}$-SWI4-GFP* was ~2 fL larger than WT diploid (Figure S4F; Table S2). These results showed that mutations that diminished the rate of Swi4 production led to a delay in Start and a larger cell size.

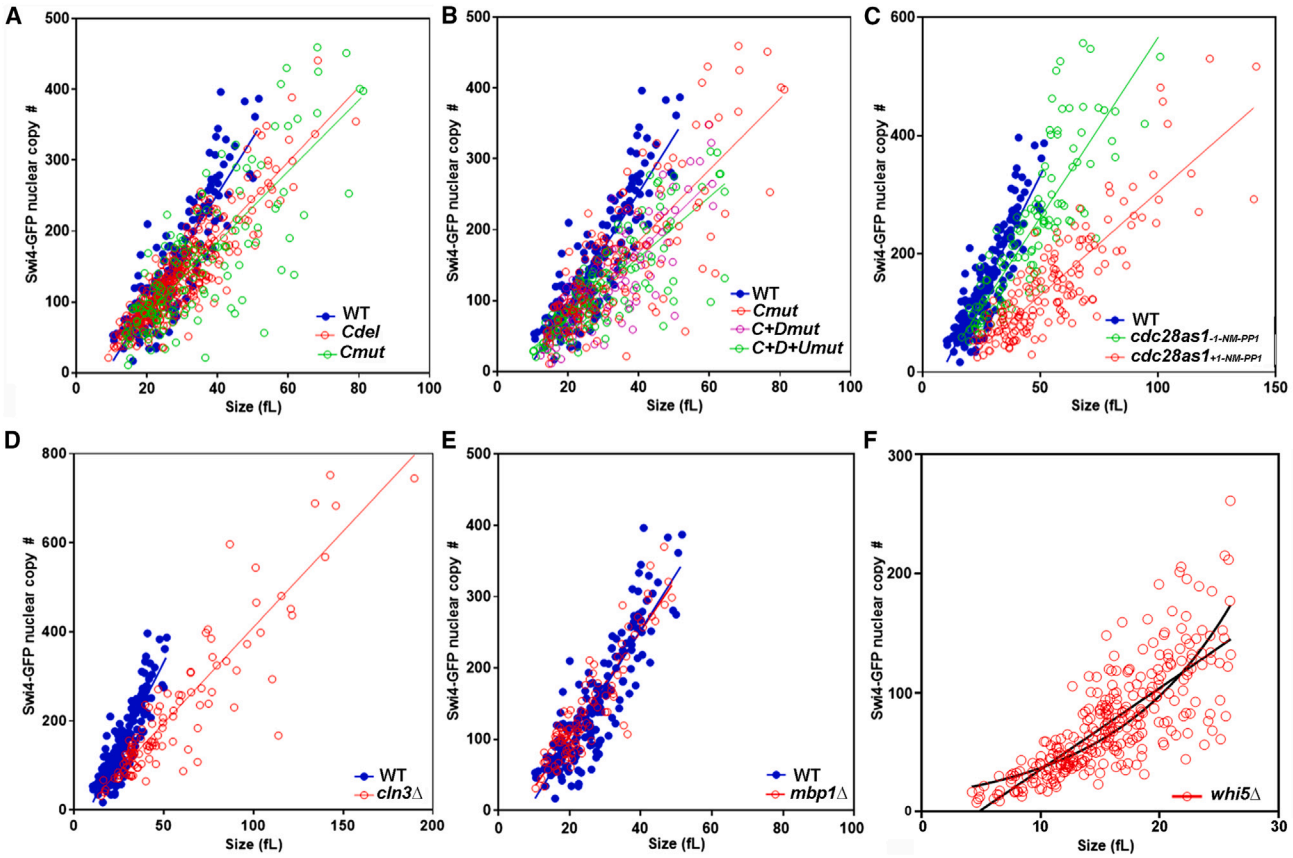

Figure 3. SCB/MCB elements in the *SWI4* promoter regulate Swi4 protein production

Nuclear copy number of Swi4-GFP as a function of cell size in (A) *SWI4-GFP* (blue), C deletion, *SWI4pr$_{Cdel}$-SWI4-GFP* (red) and C mutation, *SWI4pr$_{Cmut}$-SWI4-GFP* (green) strains; (B) *SWI4-GFP* (blue), C mutation, *SWI4pr$_{Cmut}$-SWI4-GFP* (red), C + D mutations, *SWI4pr$_{C+Dmut}$-SWI4-GFP* (pink) and C + D + U mutations, *SWI4pr$_{C+D+Umut}$-SWI4-GFP* (green) strains; (C) *SWI4-GFP* (blue), *cdc28-as1 SWI4-GFP* in absence of 1-NM-PP1 (green) and *cdcs8-as1 - 1NM-PP1 SWI4-GFP* in presence of 10 mM 1-NM-PP1 (red); (D) *SWI4-GFP* (blue) and *cln3Δ SWI4-GFP* (red); (E) *SWI4-GFP* (blue) and *mbp1Δ SWI4-GFP* (red); and (F) *SWI4-GFP* (blue) and *whi5Δ SWI4-GFP* (red). Number of cells were *SWI4-GFP* (MTy5270) 115, *SWI4pr$_{Cdel}$-SWI4-GFP* (MTy5320) 387, *SWI4pr$_{Cmut}$-SWI4-GFP* (MTy5314) 142, *SWI4pr$_{C+Dmut}$-SWI4-GFP* (MTy5298) 130, *SWI4pr$_{C+D+Umut}$-SWI4-GFP* (MTy5302) 138, *cdc28as1 SWI4-GFP* (MTy5317) in absence of 1-NM-PP1 116, and in presence of 1-NM-PP1 160, *cln3Δ SWI4-GFP* (MTy5318) 113, *mbp1Δ SWI4-GFP* (MTy5271) 101, and *whi5Δ SWI4-GFP* (MTy5180) 297. All data can be found in File S1.

Cln3-Cdc28-mediated phosphorylation is required for proper Swi4 accumulation

The dependence of Swi4 expression on SCB/MCB sites in the *SWI4* promoter indicated that SBF and/or MBF are involved in Swi4 production. Since SBF activation requires Cdc28 activity, we quantitatively evaluated the Cdc28-dependence of Swi4 accumulation. Chemical inhibition of kinase activity in a strain expressing an analog sensitive Cdc28, *cdc28-as1*,[29] with 10 μM of the inhibitor, 1-(*tert*-butyl)-3-(naphthalene-1-methyl)-1H-pyrazolo [3,4-d] pyrimidine-4-amine (1-NM-PP1) resulted in a large decrease in Swi4-GFP copy-number accumulation (56%) with respect to cell size (Figure 3C; Table 1). Hence, Cdc28 kinase activity drives approximately half of Swi4 accumulation in G1 phase. The rate of Swi4-GFP accumulation in absence of the inhibitor was slightly lower (23%) than for WT cells, perhaps due to impaired kinase activity of the Cdc28-as1 protein. We verified the requirement for G1 phase Cdc28 activity by removing Cln3, which activates Cdc28 in early G1 phase. *CLN3* deletion decreased the rate of accumulation of Swi4-GFP as a function of cell size by ∼46%, similar to the decrease observed upon mutating all MCB and SCB sites (Figure 3D; Table 1). The large size phenotype of the *CDC28-as1* and *cln3Δ* strains was apparent in the large average cell sizes observed for cells exhibiting nuclear Swi4-GFP in our sN&B images (Table 1) and in Coulter counter measurements (Figure S4E; Table 1). Taken together, these results demonstrate that Cln3-Cdc28 kinase activity contributes to about half of Swi4 accumulation in G1, suggesting that SBF activation is critical for Swi4 accumulation.

Due to the functional overlap between SBF and MBF, and the shared ability of Swi4 and Mbp1 to bind the same SCB/MCB sites,[4,5,27,30] it is in principle possible that MBF could contribute to Swi4 expression. *MBP1* deletion only slightly decreased the rate of Swi4 copy-number accumulation versus cell size (Table 1; Figure 3E), within our measurement uncertainty, suggesting that Mbp1 does not affect Swi4 production significantly. Although it

Table 1. Effect of mutations and deletions on Swi4-GFP accumulation vs. cell size

Strain	Promoter	dSwi4/dsize (copies/fL)	% decrease vs. WT haploid	Intercept	# cells	<size> (fL)
Haploid WT	WT	7.9 ± 0.3	–	−65	115	26.5
Cdel	C deleted	5.3 ± 0.1	33	−18.4	387	29.2
Cmut	C mutated	5.0 ± 0.3	37	−16.4	142	33.6
C + Dmut	C + D mutated	4.9 ± 0.3	38	−28.7	130	30.5
C + D + Umut	C + D + U mutated	4.3 ± 0.3	46	−9.2	138	30.1
mbp1Δ	WT	7.3 ± 0.3	7	−41.7	101	25.1
cln3Δ	WT	4.3 ± 0.2	46	−20.4	113	54.6
whi5Δ	WT	6.6 ± 0.4	16	−29.6	297	17.1
cdc28-as - 1-NM-PP1	WT	6.1 ± 0.4	23	−42.9	116	46.0
cdc28-as + 1-NM-PP1	WT	3.5 ± 0.2	56	−44.9	160	54.9
WT Diploid	WT	3.3 ± 0.2	58	−18.5	118	47.8
Diploid Cdel	C deleted heterozygous	2.6 ± 0.2	67	−41	109	53.4

Note that *dSwi4/dsize* is the accumulation rate of Swi4 with respect to cell size. Average size, <size>, refers to the average size of cells in the images which exhibited a nuclear Swi4-GFP signal. Note that the value of the intercept has no physical meaning, but is used, along with the slope, to calculate the Swi4 copy number for any given cell size by extrapolation.

has been found that peak *SWI4* mRNA levels decreased relative to WT upon deletion of *MBP1*,[27] we note that discordance between mRNA and protein levels has been reported for G1/S TFs, including Swi4.[31] Swi4 accumulation in a strain deleted for *WHI5* led to an apparent non-linear accumulation with respect to size (Figure 3F). However, since the improvement in the fit with an exponential model was modest, we have reported the results of the linear fit (Table 1). The lower linear Swi4 accumulation rate for the *whi5Δ* strain (20%) with respect to WT is likely due to the imperfect linear approximation. Newborn daughter *whi5Δ* cells are very small, ∼5 fL, and had only ∼14 copies of Swi4 (∼7 dimers), which is extremely sub-stoichiometric with respect to the ∼200 G1/S promoters. We note that the cell-to-cell variation in Swi4 concentration for all strains examined was much larger than the variation in Swi4 protein copy number (Figure S6). Since copy number is computed as the nuclear Swi4 concentration multiplied by the nuclear volume, this means that the stochasticity is mostly associated with the growth rates of individual cells, and not the Swi4 accumulation rate, which is more robust.

Ectopic Swi4 protein expression increases endogenous Swi4 protein levels

A prediction of Swi4-dependent *SWI4* expression is that an acute ectopic increase of Swi4 in G1 cells should stimulate endogenous *SWI4* transcription and an increase in endogenous Swi4 protein. We therefore examined the effect of ectopic expression of unlabeled Swi4 on the production of Swi4-GFP from the endogenous promoter. We constructed a strain that constitutively expresses a chimeric Z3EV transcription factor

Table 2. Predicted Swi4 copy number at Start

Strain	WT glu	WT gly	C Del	C Mut	C + D Mut	C + D + U Mut	*cln3Δ*	*whi5Δ*	*cdc28as* - 1-NM-PP1	*cdc28as* +1-NM-PP1	WT Dip	*SWI4/SWI4pr$_{Cdel}$-SWI4-GFP* Dip
Size at Start (expt)	28[a] 30[b]	23.5[a]	30[c]	33[c]	33.5[b]	34.4[c]	49[c]	22[b]	49[c]	-	48[c]	49[c]
Swi4 copies at Start[d,e]	170 ± 13	200 ± 16	140 ± 18	150 ± 21	135 ± 15	140 ± 16	190 ± 20	105 ± 20	ND	ND	190 ± 18	110 ± 24

[a]Experimental size at Start determined previously (Dorsey et al. 2018) for cells grown in SC+2% glucose or glycerol medium and expressing Whi5-GFP. Size at Start was determined based on cumulative frequency of all cells computed from Coulter Z2 Multi-sizer distributions and the fraction of pre-Start cells determined as those exhibiting nuclear Whi5-GFP using high resolution microscopy. Note that Whi5 exit is the earliest manifestation of Start, and thus the size at Start determined by this method may be a slightly smaller than that determined by other means.
[b]Taken from Jorgensen 2007.
[c]For mutant strains and diploids, the experimental size at Start was calculated as the product of WT cell size at Start in glucose medium and the ratio of median cell size of the mutant strain cells with respect to WT determined by Coulter counter measurements (Table S2).
[d]Swi4 copies within an uncertainty of 20 were calculated from the linear fits of the data in Figure 3, given in Table 1.
[e]Error on the Swi4 copy number at Start was estimated from the uncertainty in the y and x intercept from the linear fit of Swi4 copy number vs. size for the WT strain.

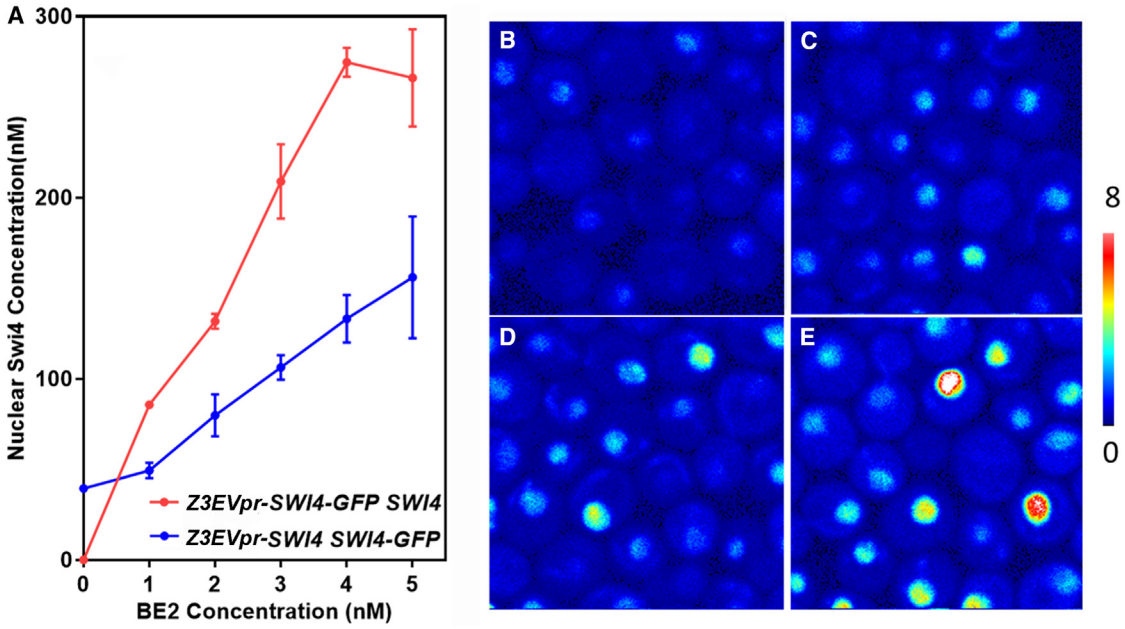

Figure 4. BE2-dependent production of Swi4-GFP

(A) Swi4-GFP nuclear concentration as a function of beta-estradiol (BE2) concentration for the P_{Z3EV}-*SWI4 SWI4-GFP* strain (MTy5189) (blue) and the control *Z3EVpr-SWI4-GFP SWI4* strain (MTy5190) (red). Nuclear concentration was calculated as the average of all cell nuclei from all FOV imaged.

(B–E) Images of FOV of the *Z3EVpr-SWI4 SWI4-GFP* strain (MTy5189) in presence of 0, 2, 3, and 5 nM BE2, respectively. Image full scale is 0–8 counts per 40 μs dwell time. Note that in absence of BE2, the average nuclear intensity was higher in the *Z3EVpr-SWI4 SWI4-GFP* strain than for the control strain due to the presence of endogenous Swi4-GFP.[19] FOV are 20 × 20 μm. Error bars represent the standard error of the mean from the value of average nuclear Swi4 concentration of all the cells between two replicates.

from the *ACT1* promoter with an additional copy of the *SWI4* gene under the control of a *Z3EV*-responsive promoter at the *BUD9* locus.[32–34] The Z3EV transcription factor is composed of the human Znf268 zinc-finger DNA binding domain, which recognizes a 9 base pair sequence, fused to the ligand binding domain of the estrogen receptor, which is responsive to beta-estradiol (BE2). Hence, the activity of this chimeric TF, and therefore the transcription of the exogenous *SWI4* gene cassette, is BE2 dependent.

In a control strain to assess BE2-dependent expression, *SWI4-GFP* was expressed from the *Z3EV* promoter in the cassette, while the endogenous copy of *SWI4* remained unlabeled (*Z3EVpr-SWI4-GFP SWI4*). We used this strain to measure how much Swi4 protein was produced by the *Z3EV* promoter as a function of BE2 concentration. BE2-dependent expression and nuclear localization of Swi4-GFP was observed as expected, with intensities of Swi4-GFP at a background level in absence of BE2 (Figures 4A and S7) and reaching saturation in presence of 5 nM BE2. We note that prolonged overexpression of Swi4-GFP in this strain upon addition of 5 nM BE2 (Figure 4A) led to cytokinesis defects (Figure S7D). This is not surprising since abnormal morphology associated with over-expression of Swi4 has been reported previously.[9]

In the experimental strain, the exogenous Swi4 expressed from the *Z3EV* promoter was unlabeled, while Swi4-GFP was expressed from the endogenous *SWI4* promoter *(Z3EVpr-SWI4 SWI4-GFP)*. We used this strain to measure how much Swi4 protein was produced by the endogenous promoter in response to ectopic Swi4 induction as a function of BE2 concentration (Figures 4A-blue and 4B–4D). We observed a substantial increase in the endogenous Swi4-GFP expression with increasing concentrations of BE2. This result confirmed a key prediction, *i.e.*, that additional ectopic Swi4 should increase endogenous Swi4-GFP expression.

Because of the cytokinesis defect, homeostatic cell size at the population level could not be used as readout for acceleration of Start in response to BE2 in the *Z3EV* strains. To directly examine the effect of Swi4 over-expression on the timing of Start, we collected small G1 daughter cells from the *Z3EVpr-SWI4 SWI4-GFP* strain synchronized by centrifugal elutriation. We then measured the time dependence of Swi4-GFP production in absence of BE2 and in presence of 5 nM BE2 (Figure 5) using imaging conditions that minimized photo-bleaching.[22] To further avoid photobleaching, each time point corresponded to a different fields of view (FOV). In presence of 5 nM BE2, the endogenous Swi4-GFP intensity increased markedly as a function of time, whereas in the absence of BE2 the signal was comparable to that observed in the WT strain expressing Swi4-GFP (Figures 5A and 5B). The WT Swi4-GFP nuclear intensity (proportional to concentration) increased by a factor of ~1.5 between birth and Start as a function of time, slightly less than observed as a function of size, ~1.8-fold.[19] This difference is likely due to the fact that the time-dependent imaging was carried out at 21°C where growth is slowed, whereas the size-dependent images are snapshots of cells growing at 30°C.

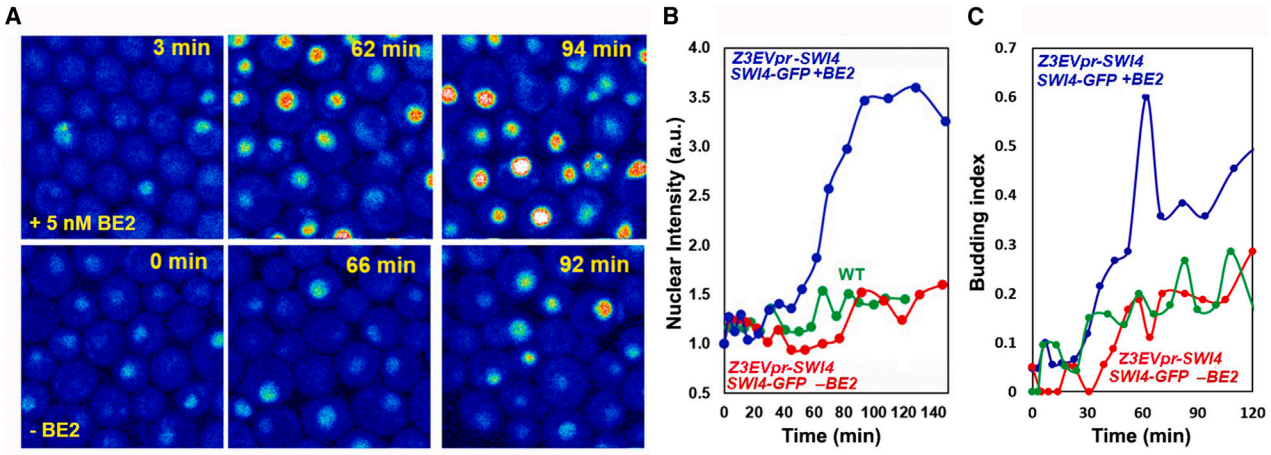

Figure 5. Effect of BE2-dependent exogenous Swi4 production on *SWI4* transcription

(A) Images of fields of view (FOV) of elutriated G1 daughter cells from the *Z3EVpr-SWI4 SWI4-GFP* strain (MTy5189) in presence of 5 nM BE2 (top row) and in absence of BE2 (bottom row), as a function of time after addition of BE2 to the top row cells. Time points are indicated in the images. Intensity scale is 0 (black) to 2 (white) photon counts per 40 μs pixel dwell-time. FOV are 20 × 20 μm.

(B) Normalized intensity of nuclear Swi4-GFP as a function of time for the *Z3EVpr-SWI4 SWI4-GFP* strain (MTy5189) in presence of 5 nM BE2 (blue), in absence of BE2 (red) and the WT Swi4-GFP strain (green). Note that the x axis is time in minutes, not size, and the y axis is average nuclear intensity (proportional to concentration), not copy number as in Figure 3).

(C) Budding index as a function of time for the *Z3EVpr-SWI4 SWI4-GFP* strain (MTy5189) strain in presence of 5 nM BE2 (blue), in absence of BE2 (red) and the WT Swi4-GFP strain (green). Cells were grown in SC+2% glucose medium. Note that cells were imaged over time on the microscope at 21°C. Average number of cells quantified per time point was 22 ± 2 for the WT Swi4-GFP time course, 19 ± 2 for the *Z3EVpr-SWI4 SWI4-GFP* strain (MTy5189) in presence of 5 nM BE2 and 20 ± 2 in absence of BE2.

Increasing Swi4 levels accelerates the timing of start

We have previously shown that Swi6 copy number in G1 phase is in excess compared to Swi4 and, moreover, that the Swi4/Whi5 ratio in WT cells grown in glucose medium depends on cell size, increasing from ∼0.42 in small cells to ∼0.84 in large G1 cells.[19] We thus expected that increased Swi4 production in response to BE2 would increase the number of active SBF complexes to levels sufficient to overcome Whi5 inhibition, leading to an acceleration of Start. In time course imaging experiments, we found that the budding index, i.e., the fraction of cells in the FOV exhibiting buds, increased more rapidly in presence of 5 nM BE2 than in its absence for the *Z3EVpr-SWI4 SWI4-GFP* strain (Figure 5C). We note that since a different FOV was imaged for each time point and because fluorescence intensity was quite low in the cytoplasm, the nascent buds were difficult to identify and hence the reported budding indices were underestimated relative to the number of actual post-Start cells (see Figure 5C in the study by Litsios A et al.[22] for a robust time dependence of post-Start cells under the same imaging conditions).

Premature budding should also correlate with an increased expression of the G1/S regulon as ectopic Swi4 accumulates. To test this hypothesis, we performed a whole-genome RNA-sequencing time course following treatment of a *Z3EVpr-SWI4* (MTy5188) strain in absence and presence of 5 nM BE2. The BE2-dependent expression of *SWI4* led to an increase in expression of several key G1/S regulon genes, including *CLN1* and *PCL1* (Figures 6A and 6B; Table S3). A number of SBF and MBF target genes were also down-regulated in a time-dependent manner, including a known MBF target, *CDC21* (Figures 6C and 6D; Table S4). These results demonstrate that ectopic production of Swi4 is sufficient to prematurely activate G1/S transcription and Start.

A threshold of Swi4 protein copy number gates Start

The aforementioned results revealed that genetic contexts that affect the critical cell size at Start also modulate the rate of Swi4 accumulation with respect to growth rate, supporting the hypothesis that a threshold in Swi4 copy number is required for Start. To test this idea further, we computed the number of Swi4 molecules present in WT cells grown in glucose medium when cells pass Start, and compared this number to the Swi4 copy number that corresponds to the estimated critical cell size at Start in other genetic/environmental conditions, given their distinct Swi4 accumulation rates with respect to growth. We previously showed that WT cells are 28 fL in size at Start based on the cumulative fraction of Whi5-GFP-containing WT cells grown in the same conditions,[19] in reasonable agreement with the size observed for onset of budding, 30 fL.[28] From the Swi4-GFP copy number versus cell size plot (Figure 3A), we estimated that WT cells grown in glucose have accumulated about 170 (±13) Swi4 molecules when they reach 28 fL and pass Start (Table 2).

Using the Swi4 accumulation rate versus cell size across genetic backgrounds (Table 2), we computed the number of Swi4 copies at Start for other strains and conditions. The size at Start was estimated from the ratio of the median daughter cell size obtained by Coulter counter measurements of the mutant strains to that of the WT strain (Table S2), multiplied by the size at Start for the WT strain (28 fL). The promoter mutant

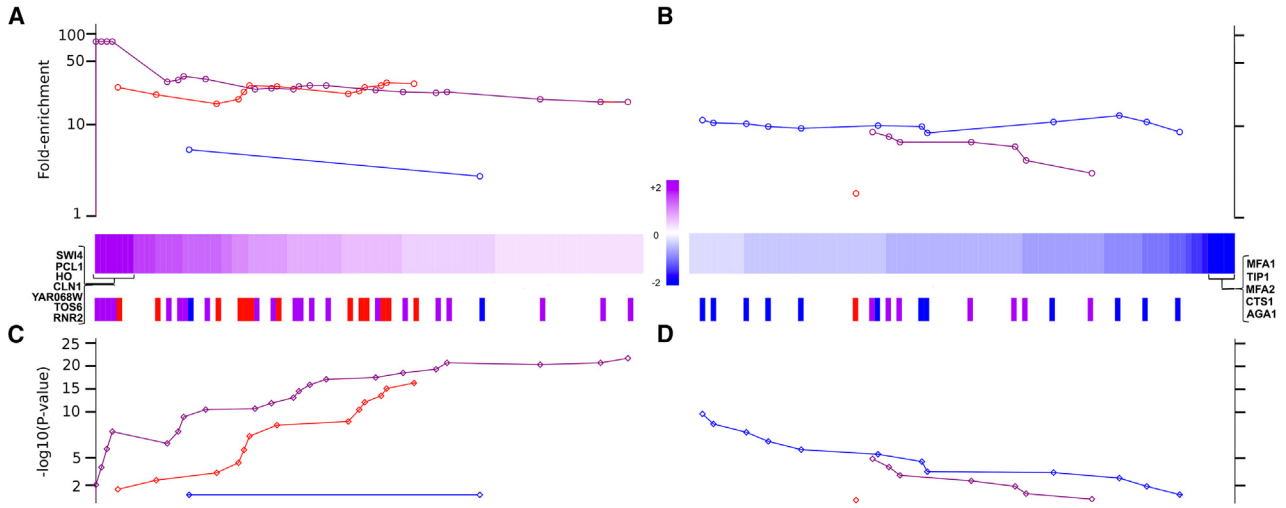

Figure 6. Effect of BE2-dependent exogenous Swi4 production on transcription of the G1/S regulon

(A and B) Cumulative fold enrichment of SBF-only (red), MBF-only (blue) or SBF and MBF (purple-pink) target genes in the top 100 most upregulated (A) or downregulated (B) genes ranked by log2 fold-change in BE2-treated compared to untreated and ethanol-treated cells. Colored strips represent the magnitude (log2 fold-change) of up-regulation (pink) and downregulation (blue) per gene. Genes with absolute log2 fold-change ≥ 1.75 are labeled on either side (the 7 most up-regulated and 5 most downregulated genes). Red, blue and purple-pink bars below the log2 fold-change strips indicate genes which are targets of SBF, MBF, or both complexes, respectively (45).

(C and D) –log10 *p* values corresponding to the cumulative enrichments shown in A (C) and B (D). A complete list of the top 100 up- and down-regulated genes and their log2 fold-changes is provided in Table S3, S4, and for all genes in SI Data File 2. Strain used was *Z3EVpr-SWI4 SWI4* (MTy5188).

strains were slightly larger than WT, with a correspondingly larger estimated size at Start (Table 2). The corresponding threshold number of Swi4 copies present in these cells at Start (Table 2) was slightly lower than for WT cells, but within the uncertainty as deduced from the linear fit of the plot of WT Swi4 copy number vs. size (Figure 4). For diploid cells, based on the measured Swi4 accumulation rate (Table 1), 190 ± 18 Swi4 molecules per genome were predicted at the estimated size at Start of 48 fL. This Swi4 copy number at Start value was also within the uncertainty of that found for haploid cells (170 ± 13). Thus, the lower Swi4 accumulation rate per haploid genome in diploid cells (Table 1), whatever its origin (see discussion), accounts reasonably well for the relationship between size and ploidy. Likewise, using our prior results for Swi4 copy number accumulation versus size for WT haploid cells grown in glycerol,[19] a Swi4 copy number of 200 ± 16 predicted a size at Start of 23 ± 2 fL. While the Swi4 copy number at Start is slightly higher than in glucose, it is within the uncertainty of our measurements, and the predicted size is quite close to the previously measured value of 23.5 fL.[19] Based on the concordance of the number of copies of Swi4 at Start in these strains and conditions, we propose that a required threshold of approximately 170 ± 20 Swi4 molecules per haploid genome gates Start across the tested strains and conditions.

This threshold of ~170 ± 20 Swi4 copies was determined earlier for strains in which the phosphorylation module of the G1/S regulatory network is intact. We next calculated the Swi4 copy number present at Start for the *cln3Δ* strain in which SBF-Whi5 phosphorylation is compromised. The experimental size at Start for the *cln3Δ* strain, estimated as above (Table 2; refer the study by Adames N.R. et al[35]), is 49 fL. Based on the linear fit for Swi4 accumulation in this strain (Table 1), the Swi4 copy number at Start was 190 ± 20, within the uncertainty of the estimated threshold value for WT. Note that the proportion of cells in G1 phase is ~7% larger in the *cln3Δ* strain relative to WT,[36] such that the size at Start, and thus, the corresponding Swi4 copy number, could be 7% larger than 190 (~200), still in reasonable agreement with the WT threshold. In the *whi5Δ* strain, cells passed Start at a smaller size, estimated at 22 fL (Table S2, refer the study by Jorgensen P et al.[11]). This size corresponded to a substantially lower Swi4 copy number, 105 ± 20 (Figure 3; Table 1), compared to the ~170 ± 20 found for WT. Hence, *whi5Δ* cells, in which all SBF complexes are de-repressed, pass Start with significantly fewer copies of Swi4 than WT cells, suggesting that fewer but more active SBF complexes may reduce the threshold requirement for Swi4 copy number at Start.

DISCUSSION

The role of Swi4-dependent *SWI4* transcription in the Start transition is supported by four main lines of evidence: (1) quantitative sN&B measurements show that the rate of accumulation of Swi4 versus size depends on the presence of Swi4 target sites in the *SWI4* promoter; (2) dependence of Swi4 accumulation rate on Cln3-Cdc28 activity; (3) ectopic Swi4-mediated induction of endogenous Swi4 expression and acceleration of G1/S transcription; (4) decreased rate of Swi4 accumulation in diploids with respect to growth and concomitantly larger cell size. Swi4-dependent *SWI4* transcription is responsible for approximately half of Swi4 accumulation in G1 phase in WT haploid cells grown in glucose medium. Interestingly, the contribution of *SWI4* autoregulation to Swi4 accumulation corresponds to

the difference in accumulation rate of Swi4 with respect to that of the other G1/S TFs (Swi6, Whi5, and Mbp1), all of which scale approximately linearly with growth and exhibit size-independent concentrations.[19] The interconnected feedback loops of Swi4 production, Cln1/2 production,[18] and SBF/Whi5 phosphorylation[12,13,37] all combine to drive a size-resolved, sharp and effectively irreversible Start transition.

Our current and previous experimental quantification[19,23] revealed that nuclear Swi4 copy number is quite low in small cells grown in rich medium (~35 molecules—well below the number of target 200 G1/S promoters) and increases as cells grow, reaching a level of ~170 molecules at the point when cells pass Start at ~30 fL. In comparison, immunoblot-based quantification yielded 589 Swi4 copies per cell.[38] The absolute abundance (copy number/cell) of Swi4 has been determined by mass spectrometry (MS) in several studies, with values differing by over an order of magnitude from 195[39] to 1,334–4,893 (depending on replicates)[40] to 2,655 copies.[41] Our results based on sN&B are in closest agreement with the results of in-StageTip MS using encapsulated processing, which likely avoids contamination and other processing errors.[39] Other MS-based protein quantification studies in yeast failed to report values for Swi4, consistent with low abundance.[42,43] A meta-analysis study based on either MS or standard epi-fluorescence microscopy data, in which Swi4 abundance originally reported in arbitrary units were converted to absolute copy numbers using re-normalization approaches,[44] yielded Swi4 copy numbers of 925 (MS data from the study by Webb K.J. et al.[45]), 1,169 (MS data from the study by Thakur S.S. et al.[46]), 1,387 (MS data from the study by Nagraj N. et al.[47]), 1,487 (MS data from the study by De Godoy et al.[48]), 1,595 (fluorescence data from the study by Breker M. et al.[49]),or ~1,800 (fluorescence data from the study by Tkach J.M. et al.[50]). This meta-analysis concluded that MS is more sensitive than simple epi-fluorescence for detection of low abundance proteins (<1,400 copies per cell), due to cellular autofluorescence overwhelming weak signals from fluorescently tagged proteins of interest, but also that MS based measurements were more variable than fluorescence-based measurements.[44] We emphasize that low perturbation 2-photon fluorescence fluctuation microscopy combines both sensitivity (very low autofluorescence with an excitation wavelength of 1 μm) and accuracy for determining molecular concentrations in solution or in cells.[51,52] Our calibration-based sN&B method, which relies on average, autofluorescence-corrected fluorescence intensity and a precisely determined value for the molecular brightness of GFP, is even more robust and reproducible,[19] in addition to being a single-cell technique that captures variability and correlations with single cell phenotypes.

The growth-dependent increase in Swi4 copy number reported previously[19,23] and in the present work suggests that increasing G1/S TF copy number is required to titrate G1/S promoters to enable Start. This hypothesis of promoter titration by Swi4 is reminiscent of previous titration models, notably titration of G1/S promoters by Cln3,[53] the DNA titration-based differential scaling of histone production,[54] DnaA accumulation in replication initiation in *E. coli*,[55] and even earlier work on the myxomycete, *P. plycephalum*, for which synchronous mitosis appeared to be triggered by the accumulation of a specific protein in the cytoplasm.[56] The observations reported here add substantial additional experimental evidence in support of the Swi4 titration model, reveal positive feedback for Swi4 accumulation, and quantify the Swi4 threshold for Start. Our Swi4 measurements suggest that in wild type cells, a threshold of ~170 ± 20 Swi4 monomers is required to activate Start. This Swi4 threshold accounts reasonably well for the difference in cell size for diploids compared to haploids and the effects of mutations in the *SWI4* promoter (Figure 7A). The promoter titration model also rationalizes the small size at Start of WT cells grown in poor nutrients, due to the positive differential scaling of Swi4 accumulation with respect to growth. Moreover, within experimental uncertainty, the Swi4 threshold accounts for the observed size at Start for the promoter mutant strains and the *cln3Δ* strain (Figure 7B). We do not rule out contributions to Start from other factors and, indeed, it would be surprising if additional mechanisms did not govern size as a critical attribute of cell fitness. Nonetheless, the posited Swi4 copy-number threshold accounts reasonably well for the observed size phenotypes.

We have shown previously that the stoichiometry of nuclear complexes containing either Swi4 or Swi6 is two copies of Swi4/Swi6 monomers per complex, indicating that SBF complexes are on average hetero-tetramers (i.e., $(Swi4)_2(Swi6)_2$).[19] The threshold SBF copy number of ~170 monomers would correspond to ~85 SBF hetero-tetrameric complexes, although this is an upper limit, since we showed as well that the total Swi6 copy number is slightly lower than the total Mbp1+Swi4 copy number in cells of all sizes.[19] This number of SBF complexes (~85) is sub-saturating with respect to the ~200 promoters in the G1/S regulon, suggesting that titration of only a fraction of G1/S promoters may be required for Start, consistent with the observation that occupation of G1/S promoters is in dynamic equilibrium.[23] Previously, we found that all of the G1/S TFs (Swi4, Mbp1, Swi6, and Whi5) were present mostly in small clusters (containing ~8 copies of each protein) in the nucleus and that the number of clusters increased with the accumulation of G1/S copy number as cells grew in G1 phase, while the size of the clusters remained constant.[23] Live cell-single molecule PALM tracking experiments showed that individual proteins could dissociate from clusters on the timescale of ~100 ms and rebind to other clusters.[23] Thus, 85 SBF complexes, only a fraction of which might be active, could in principle be sufficient to activate several genes within or even among clusters.

Titration of G1/S promoters, while necessary, is not sufficient to trigger Start, as evidenced by the behavior of the analog sensitive *cdc28-as1* strain in presence of 1-NM-PP1 inhibitor,[29] which accumulates Swi4 to WT levels, yet never passes Start. Thus, the Start transition requires not only that a given fraction of the G1/S promoters be bound by SBF, but also that some fraction of the bound SBF complexes be *active.* Hence, promoter titration by SBF and SBF/Whi5 phosphorylation combine to achieve a threshold number of active SBF complexes required to pass Start. A decrease in phosphorylation activity by mutation (e.g., in a *cln3Δ* strain) results in a decreased rate of Swi4 accumulation with respect to size, and therefore, an increase in cell size at the required threshold of Swi4 molecules. Consistent with this *CLN3* dependence of *SWI4* expression, a burst of *CLN3* expression was previously shown to induce expression of *SWI4*.[16] Apparently, in this case, sufficient phosphorylation

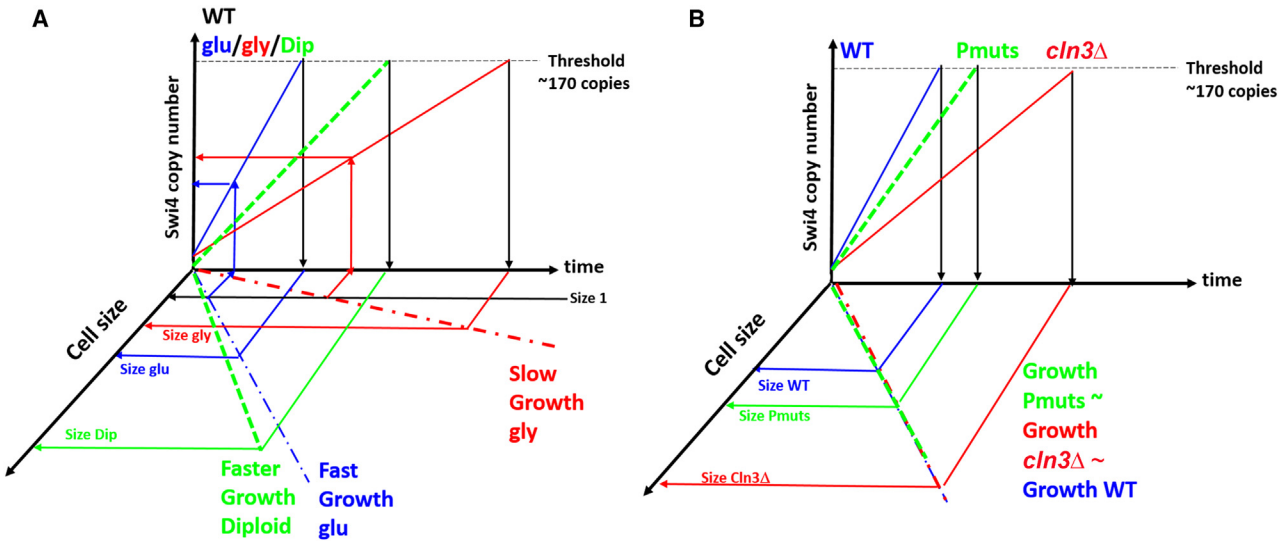

Figure 7. Schematic representation of the Swi4 threshold model

The z axis is the Swi4 monomer copy number, x axis is time and y axis is cell size. The lines in the x-y plan represent size vs. time (= growth rate), while the lines in the z-x plane represent the Swi4 copy-number accumulation rate. A required threshold of ~170 copies of Swi4 is represented by a dashed black line. Black downward arrows mark the time at which the Swi4 threshold is reached. This time corresponds to a particular cell size (given the growth rate), and hence the size at Start.

(A) Comparison of WT haploids grown in glucose (blue lines) and glycerol (red lines) and WT diploids grown in glucose (green lines). Swi4 copy number accumulation is fastest in WT haploids grown in glucose, half as fast (as observed experimentally) for WT diploids grown in glucose and very slow for WT haploids grown in glycerol. Growth is represented as being a bit faster for diploids than haploids both grown in glucose, but extremely slow for haploids grown in glycerol. Thus, glycerol slows growth more than it slows Swi4 accumulation, positive differential scaling of Swi4 copy number accumulation with respect to growth, such that cells grown in glycerol have grown less than those grown in glucose when the threshold of 170 Swi4 copies is reached. Likewise, for cells of any given size (Size 1) there are more copies of Swi4 in glycerol than in glucose, as reported in the study by Dorsey S et al.[19] In contrast, diploids accumulate Swi4 at half the rate (per genome) as haploids (as observed here), and grow a bit faster, such that diploid cells grow much larger before reaching the threshold of 170 Swi4 monomers.

(B) Comparison of WT, *cln3Δ* (red lines), and the promoter mutants (Prmuts; green lines). All growth rates are approximately the same, but the accumulation rates are slower for the mutant strains, such that the mutant strains have grown more by the time the Swi4 threshold is reached.

activity by Cln1/2-Cdc28 complex is achieved eventually when *cln3Δ* cells attain the WT Swi4 copy-number threshold to activate the fraction of SBF required for Start.

In contrast, in absence of Whi5 repression, cells pass Start at a smaller size[11] and at a lower Swi4 threshold than WT cells because SBF is not inhibited by Whi5. The number of Swi4 molecules at Start in *whi5Δ* cells (~110 monomers ~50–55 SBF hetero-tetramers) may correspond to the required threshold of active SBF complexes in WT cells. However, we cannot exclude that in *whi5Δ* cells Swi6 may also be limiting with respect to the total number of Mbp1+Swi4 molecules (as in WT cells,[19]), such that the estimated 55 active SBF complexes may represent an upper limit. Moreover, there may be a requirement for Swi6 phosphorylation, even in absence of Whi5, to achieve complete activation of SBF.[13] Indeed, cells that over-express Cln3 are smaller than *whi5Δ* cells.[57,58] Interestingly, the inherent positive feedback in Swi4 production appears to be unmasked in the *whi5Δ* strain, as Swi4 accumulation appears to be somewhat supra-linear in this case, whereas it is linear in all cases in which Whi5 phosphorylation is required. While WT Whi5 levels repress most SBF copies and therefore render the amount of active SBF only weakly dependent on the amount of available Swi4, in absence of Whi5 more Swi4 molecules immediately lead to more active SBF copies and therefore to an increase in the rate of Swi4 accumulation, yielding a supra-linear (possibly exponential) increase of Swi4 copy number with cell size. This observation suggests that in WT cells, the phosphorylation requirement hinders Swi4 positive feedback.

While we have demonstrated that differential scaling of Swi4 accumulation with respect to growth modulates cell size at Start, the molecular mechanisms responsible for this phenomenon remain to be determined. For example, why does the Swi4 accumulation rate slow less than bulk growth rate in poor nutrients? And similarly, while the observed lower Swi4 accumulation rate in diploids may account for the size relationships of ploidy, the molecular mechanism for this reduced accumulation rate per haploid genome in diploids remains to be discovered. Overall, the linked Swi4 accumulation/phosphorylation feedback loops provide distinct molecular inputs for modulation of cell size in response to mutations or growth conditions, and combined, lead to a sharp G1/S transition. Irreversible switch-like transitions are implicated in many important cellular processes, such as development, differentiation, and damage responses. Transcription factor autoregulation and titration of target promoters in complex regulons, such as that reported here, may be a recurrent regulatory motif in many of these transitions.

Limitations of the study

The threshold model proposed here has been tested only for genetic backgrounds in which genes encoding the major factors

(*CDC28*, *CLN3*, *WHI5*, and *MBP1*) implicated in Start have been mutated or deleted. Moreover, only selected nutrient conditions have been tested.

RESOURCE AVAILABILITY

Lead contact

Further information and requests for resources and reagents should be directed to and will be fulfilled by the lead contact, Catherine A. Royer (royerc@rpi.edu).

Materials availability

All strains will be provided by MT and ST pending scientific review and a completed material transfer agreement. Requests for the strains should be submitted to quantcellbiolconsulting@gmail.com or mike.tyers@sickkids.ca.

Data and code availability

- Data: GEO RNASeq data have been deposited at https://www.ncbi.nlm.nih.gov/geo/ (accession number GSE279708) and are publicly available as of the date of publication. All other data needed to evaluate the conclusions in the paper are present in the paper and/or the Supplementary Materials or Supplementary Files. Raw imaging data will be made available upon request.
- Code: In addition to the commercial software referenced in the Key Resource Table, custom MATLAB scripts were used to analyze the data in Figure 3. These scripts are available upon request.

ACKNOWLEDGMENTS

This work was supported by grants Canadian Institutes of Health Research FDN-167277 to M.T., the Academy of Finland (grant #350887) and the Sigrid Jusélius Foundation (grant #220196) to S.T. and NSF PHY 1806638 to C.A.R. We thank Bruce Futcher for kindly providing plasmid pGZ110, and Brenda Andrews, Jackie Vogel, and Scott McIsaac for generously providing yeast strains. We also thank anonymous reviewers for critical comments.

AUTHOR CONTRIBUTIONS

Investigation, P.G., A.G., C.C., J.C., G.G., Y.T., M.F.G., and S.T.; formal analysis, P.G., A.G., C.C., J.C.-H.; resources, J.C., G.G., and S.T.; data curation, J.C.-H., C.A.R., and A.G.; methodology, C.A.R., S.T., and M.T.; validation, G.G., J.C., and S.T.; conceptualization, S.T., M.T., and C.A.R.; software, S.T., C.A.R., J.C.-H.; writing – original draft, S.T., M.T., C.A.R., A.G., J.C., and J.C.-H.; writing – review and editing, S.T., M.T., and C.A.R.; project administration, S.T., M.T., and C.A.R.; funding acquisition, S.T., M.T., and C.A.R.

DECLARATION OF INTERESTS

The authors declare no competing interests.

STAR★METHODS

Detailed methods are provided in the online version of this paper and include the following:

- KEY RESOURCES TABLE
- EXPERIMENTAL MODEL AND STUDY PARTICIPANT DETAILS
  - Yeast strain construction
  - Experimental design
- METHOD DETAILS
  - Cell culture
  - Preparation of agarose pads
  - Elutriation of BE2-dependent strains
  - Scanning number and brightness (sN&B) imaging
  - Steady-state and time course imaging of BE2-dependent strains
  - Coulter counter cell sizing and growth curve
  - RNA-seq
- QUANTIFICATION AND STATISTICAL ANALYSIS
  - Scanning number and brightness image analysis
  - Intensity analysis
  - RNA-seq analysis

SUPPLEMENTAL INFORMATION

Supplemental information can be found online at https://doi.org/10.1016/j.isci.2025.112027.

Received: April 24, 2024
Revised: August 22, 2024
Accepted: February 11, 2025
Published: February 13, 2025

REFERENCES

1. Bertoli, C., Skotheim, J.M., and De Bruin, R.A.M. (2013). Control of cell cycle transcription during G1 and S phases. Nat. Rev. Mol. Cell Biol. *14*, 518–528. https://doi.org/10.1038/nrm3629.
2. DeGregori, J., Kowalik, T., and Nevins, J.R. (1995). Cellular Targets for Activation by the E2F1 Transcription Factor Include DNA Synthesis- and G 1/S-Regulatory Genes. Mol. Cell Biol. *15*, 4215–4224. https://doi.org/10.1128/mcb.15.8.4215.
3. Koch, C., Moll, T., Neuberg, M., Ahorn, H., and Nasmyth, K. (1993). A role for the transcription factors Mbp1 and Swi4 in progression from G1 to S phase. Science *261*, 1551–1557. https://doi.org/10.1126/science.8372350.
4. Iyer, V.R., Horak, C.E., Scafe, C.S., Botstein, D., Snyder, M., and Brown, P.O. (2001). Genomic binding sites of the yeast cell-cycle transcription factors SBF and MBF. Nature *409*, 533–538. https://doi.org/10.1038/35054095.
5. Bean, J.M., Siggia, E.D., and Cross, F.R. (2005). High functional overlap between MluI cell-cycle box binding factor and Swi4/6 cell-cycle box binding factor in the G1/S transcriptional program in Saccharomyces cerevisiae. Genetics *171*, 49–61. https://doi.org/10.1534/genetics.105.044560.
6. Jorgensen, P., Rupeš, I., Sharom, J.R., Schneper, L., Broach, J.R., and Tyers, M. (2004). A dynamic transcriptional network communicates growth potential to ribosome synthesis and critical cell size. Genes Dev. *18*, 2491–2505. https://doi.org/10.1101/gad.1228804.
7. Nasmyth, K., and Dirick, L. (1991). The role of SWI4 and SWI6 in the activity of G1 cyclins in yeast. Cell *66*, 995–1013. https://doi.org/10.1016/0092-8674(91)90444-4.
8. Primig, M., Sockananthan, S., Auer, H., and Nasmyth, K. (1992). Anatomy of a transcription factor important for the Start of the cell cycle in Saccharomycs cerevisiae. Nature *355*, 242–244. https://doi.org/10.1038/355242a0.
9. Breeden, L., and Mikesell, G.E. (1991). Cell cycle-specific expression of the SWI4 transcription factor is required for the cell cycle regulation of HO transcription. Genes Dev. *5*, 1183–1190.
10. McInerny, C.J., Partridge, J.F., Mikesell, G.E., Creemer, D.P., and Breeden, L.L. (1997). A novel Mcm1-dependent element in the SWI4, CLN3, CDC6, and CDC47 promoters activates M/G1-specific transcription. Genes Dev. *11*, 1277–1288. https://doi.org/10.1101/gad.11.10.1277.
11. Jorgensen, P., Nishikawa, J.L., Breitkreutz, B.-J., and Tyers, M. (2002). Systematic identification of pathways that couple cell growth and division in yeast. Science *297*, 395–400. https://doi.org/10.1126/science.1070850.
12. de Bruin, R.A.M., McDonald, W.H., Kalashnikova, T.I., Yates, J., and Wittenberg, C. (2004). Cln3 activates G1-specific transcription via phosphorylation of the SBF bound repressor Whi5. Cell *117*, 887–898. https://doi.org/10.1016/j.cell.2004.05.025.
13. Costanzo, M., Nishikawa, J.L., Tang, X., Millman, J.S., Schub, O., Breitkreuz, K., Dewar, D., Rupes, I., Andrews, B., and Tyers, M. (2004). CDK

activity antagonizes Whi5, an inhibitor of G1/S transcription in yeast. Cell *117*, 899–913. https://doi.org/10.1016/j.cell.2004.05.024.

14. Richardson, H.E., Wittenberg, C., Cross, F., and Reed, S.I. (1989). An essential G1 function for cyclin-like proteins in yeast. Cell *59*, 1127–1133. https://doi.org/10.1016/0092-8674(89)90768-X.
15. Neurohr, G.E., Terry, R.L., Lengefeld, J., Bonney, M., Brittingham, G.P., Moretto, F., Miettinen, T.P., Vaites, L.P., Soares, L.M., Paulo, J.A., et al. (2019). Excessive Cell Growth Causes Cytoplasm Dilution And Contributes to Senescence. Cell *176*, 1083–1097. https://doi.org/10.1016/j.cell.2019.01.018.
16. Tyers, M., Tokiwa, G., and Futcher, B. (1993). Comparison of the Saccharomyces cerevisiae G1 cyclins: Cln3 may be an upstream activator of Cln1, Cln2 and other cyclins. EMBO J. *12*, 1955–1968.
17. Litsios, A., Huberts, D.H.E.W., Terpstra, H.M., Guerra, P., Schmidt, A., Buczak, K., Papagiannakis, A., Rovetta, M., Hekelaar, J., Hubmann, G., et al. (2019). Differential scaling between G1 protein production and cell size dynamics promotes commitment to the cell division cycle in budding yeast. Nat. Cell Biol. *21*, 1382–1392. https://doi.org/10.1038/s41556-019-0413-3.
18. Skotheim, J.M., Di Talia, S., Siggia, E.D., and Cross, F.R. (2008). Positive feedback of G1 cyclins ensures coherent cell cycle entry. Nature *454*, 291–296. https://doi.org/10.1038/nature07118.
19. Dorsey, S., Tollis, S., Cheng, J., Black, L., Notley, S., Tyers, M., and Royer, C.A. (2018). G1/S Transcription Factor Copy Number Is a Growth-Dependent Determinant of Cell Cycle Commitment in Yeast. Cell Syst. *6*, 539–554. https://doi.org/10.1016/j.cels.2018.04.012.
20. Schmoller, K.M., Turner, J.J., Kõivomägi, M., and Skotheim, J.M. (2015). Dilution of the cell cycle inhibitor Whi5 controls budding-yeast cell size. Nature *526*, 268–272. https://doi.org/10.1038/nature14908.
21. Schmoller, K.M., Lanz, M.C., Kim, J., Koivomagi, M., Qu, Y., Tang, C., Kukhtevich, I.V., Schneider, R., Rudolf, F., Moreno, D.F., et al. (2022). Whi5 is diluted and protein synthesis does not dramatically increase in pre-Start G1. Mol. Biol. Cell *33*, lt1. https://doi.org/10.1091/mbc.E21-01-0029.
22. Litsios, A., Goswami, P., Terpstra, H.M., Coffin, C., Vuillemenot, L.A., Rovetta, M., Ghazal, G., Guerra, P., Buczak, K., Schmidt, A., et al. (2022). The timing of Start is determined primarily by increased synthesis of the Cln3 activator rather than dilution of the Whi5 inhibitor. Mol. Biol. Cell *33*, rp2. https://doi.org/10.1091/mbc.E21-07-0349.
23. Black, L., Tollis, S., Fu, G., Fiche, J.B., Dorsey, S., Cheng, J., Ghazal, G., Notley, S., Crevier, B., Bigness, J., et al. (2020). G1/S transcription factors assemble in increasing numbers of discrete clusters through G1 phase. J. Cell Biol. *219*, e202003041. https://doi.org/10.1083/JCB.202003041.
24. Foster, R., Mikesell, G.E., and Breeden, L. (1993). Multiple SWI6-Dependent cis-Acting Elements Control SWI4 Transcription through the Cell Cycle. Mol. Cell Biol. *13*, 3792–3801.
25. Simon, I., Barnett, J., Hannett, N., Harbison, C.T., Rinaldi, N.J., Volkert, T.L., Wyrick, J.J., Zeitlinger, J., Gifford, D.K., Jaakkola, T.S., and Young, R.A. (2001). Serial regulation of transcriptional regulators in the yeast cell cycle. Cell *106*, 697–708. https://doi.org/10.1016/S0092-8674(01)00494-9.
26. MacKay, V.L., Mai, B., Waters, L., and Breeden, L.L. (2001). Early Cell Cycle Box-Mediated Transcription of CLN3 and SWI4 Contributes to the Proper Timing of the G 1 -to-S Transition in Budding Yeast. Mol. Cell Biol. *21*, 4140–4148. https://doi.org/10.1128/mcb.21.13.4140-4148.2001.
27. Harris, M.R., Lee, D., Farmer, S., Lowndes, N.F., and de Bruin, R.A.M. (2013). Binding Specificity of the G1/S Transcriptional Regulators in Budding Yeast. PLoS One *8*, 610599. https://doi.org/10.1371/journal.pone.0061059.
28. Jorgensen, P., Edgington, N.P., Schneider, B.L., Rupeš, I., Tyers, M., and Futcher, B. (2007). The size of the nucleus increases as yeast cells grow. Mol. Biol. Cell *18*, 3523–3532.
29. Bishop, A.C., Ubersax, J. a, Petsch, D.T., Matheos, D.P., Gray, N.S., Blethrow, J., Shimizu, E., Tsien, J.Z., Schultz, P.G., Rose, M.D., et al. (2000). A chemical switch for inhibitor-sensitive alleles of any protein kinase. Nature *407*, 395–401. https://doi.org/10.1038/35030148.
30. Bastos de Oliveira, F.M., Harris, M.R., Brazauskas, P., de Bruin, R. a M., and Smolka, M.B. (2012). Linking DNA replication checkpoint to MBF cell-cycle transcription reveals a distinct class of G1/S genes. EMBO J. *31*, 1798–1810. https://doi.org/10.1038/emboj.2012.27.
31. Kelliher, C.M., Foster, M.W., Motta, F.C., Deckard, A., Soderblom, E.J., Moseley, M.A., and Haase, S.B. (2018). Layers of regulation of cell-cycle gene expression in the budding yeast Saccharomyces cerevisiae. Mol. Biol. Cell *29*, 2644–2655. https://doi.org/10.1091/mbc.E18-04-0255.
32. Arita, Y., Kim, G., Li, Z., Friesen, H., Turco, G., Wang, R.Y., Climie, D., Usaj, M., Hotz, M., Stoops, E.H., et al. (2021). A genome-scale yeast library with inducible expression of individual genes. Mol. Syst. Biol. *17*, e10207. https://doi.org/10.15252/msb.202110207.
33. McIsaac, R.S., Oakes, B.L., Wang, X., Dummit, K.A., Botstein, D., and Noyes, M.B. (2013). Synthetic gene expression perturbation systems with rapid, tunable, single-gene specificity in yeast. Nucleic Acids Res. *41*, e57. https://doi.org/10.1093/nar/gks1313.
34. McIsaac, R.S., Gibney, P.A., Chandran, S.S., Benjamin, K.R., and Botstein, D. (2014). Synthetic biology tools for programming gene expression without nutritional perturbations in Saccharomyces cerevisiae. Nucleic Acids Res. *42*, e48-8. https://doi.org/10.1093/nar/gkt1402.
35. Adames, N.R., Schuck, P.L., Chen, K.C., Murali, T.M., Tyson, J.J., and Peccoud, J. (2015). Experimental testing of a new integrated model of the budding yeast Start transition. Mol. Biol. Cell *26*, 3966–3984. https://doi.org/10.1091/mbc.E15-06-0358.
36. Teufel, L., Tummler, K., Flöttmann, M., Herrmann, A., Barkai, N., and Klipp, E. (2019). A transcriptome-wide analysis deciphers distinct roles of G1 cyclins in temporal organization of the yeast cell cycle. Sci. Rep. *9*, 1–14. https://doi.org/10.1038/s41598-019-39850-7.
37. Wagner, M.V., Smolka, M.B., de Bruin, R.A.M., Zhou, H., Wittenberg, C., and Dowdy, S.F. (2009). Whi5 regulation by site specific CDK-phosphorylation in Saccharomyces cerevisiae. PLoS One *4*, e4300–e430012. https://doi.org/10.1371/journal.pone.0004300.
38. Ghaemmaghami, S., Huh, W.K., Bower, K., Howson, R.W., Belle, A., Dephoure, N., O'Shea, E.K., and Weissman, J.S. (2003). Global analysis of protein expression in yeast. Nature *425*, 737–741.
39. Kulak, N. a, Pichler, G., Paron, I., Nagaraj, N., and Mann, M. (2014). Minimal, encapsulated proteomic-sample processing applied to copy-number estimation in eukaryotic cells. Nat. Methods *11*, 319–324. https://doi.org/10.1038/nmeth.2834.
40. Peng, M., Taouatas, N., Cappadona, S., Van Breukelen, B., Mohammed, S., Scholten, A., and Heck, A.J.R. (2012). Protease bias in absolute protein quantitation. Nat. Methods *9*, 524–525. https://doi.org/10.1038/nmeth.2031.
41. Lu, P., Vogel, C., Wang, R., Yao, X., and Marcotte, E.M. (2007). Absolute protein expression profiling estimates the relative contributions of transcriptional and translational regulation. Nat. Biotechnol. *25*, 117–124. https://doi.org/10.1038/nbt1270.
42. Lawless, C., Holman, S.W., Brownridge, P., Lanthaler, K., Harman, V.M., Watkins, R., Hammond, D.E., Miller, R.L., Sims, P.F.G., Grant, C.M., et al. (2016). Direct and absolute quantification of over 1800 yeast proteins via selected reaction monitoring. Mol. Cell. Proteomics *15*, 1309–1322. https://doi.org/10.1074/mcp.M115.054288.
43. Lahtvee, P.J., Sánchez, B.J., Smialowska, A., Kasvandik, S., Elsemman, I.E., Gatto, F., and Nielsen, J. (2017). Absolute Quantification of Protein and mRNA Abundances Demonstrate Variability in Gene-Specific Translation Efficiency in Yeast. Cell Syst. *4*, 495–504. https://doi.org/10.1016/j.cels.2017.03.003.
44. Ho, B., Baryshnikova, A., and Brown, G.W. (2018). Unification of Protein Abundance Datasets Yields a Quantitative Saccharomyces cerevisiae

Proteome. Cell Syst. *6*, 192–205. https://doi.org/10.1016/j.cels.2017.12.004.

45. Webb, K.J., Xu, T., Park, S.K., and Yates, J.R. (2013). Modified MuDPIT Separation Identified 4488 Proteins in a System-wide Analysis of Quiescence in Yeast. J. Proteome Res. *12*, 2177–2184.
46. Thakur, S.S., Geiger, T., Chatterjee, B., Bandilla, P., Fröhlich, F., Cox, J., and Mann, M. (2011). Deep and highly sensitive proteome coverage by LC-MS/MS without prefractionation. Mol. Cell. Proteomics *10*, M110.003699. https://doi.org/10.1074/mcp.M110.003699.
47. Nagaraj, N., Kulak, N.A., Cox, J., Neuhauser, N., Mayr, K., Hoerning, O., Vorm, O., and Mann, M. (2012). System-wide perturbation analysis with nearly complete coverage of the yeast proteome by single-shot ultra HPLC runs on a bench top orbitrap. Mol. Cell. Proteomics *11*, 013722. https://doi.org/10.1074/mcp.M111.013722.
48. De Godoy, L.M.F., Olsen, J.V., Cox, J., Nielsen, M.L., Hubner, N.C., Fröhlich, F., Walther, T.C., and Mann, M. (2008). Comprehensive mass-spectrometry-based proteome quantification of haploid versus diploid yeast. Nature *455*, 1251–1254. https://doi.org/10.1038/nature07341.
49. Breker, M., Gymrek, M., and Schuldiner, M. (2013). A novel single-cell screening platform reveals proteome plasticity during yeast stress responses. J. Cell Biol. *200*, 839–850. https://doi.org/10.1083/jcb.201301120.
50. Tkach, J.M., Yimit, A., Lee, A.Y., Riffle, M., Costanzo, M., Jaschob, D., Hendry, J.A., Ou, J., Moffat, J., Boone, C., et al. (2012). Dissecting DNA damage response pathways by analysing protein localization and abundance changes during DNA replication stress. Nat. Cell Biol. *14*, 966–976. https://doi.org/10.1038/ncb2549.
51. Charier, S., Meglio, A., Alcor, D., Cogné-Laage, E., Allemand, J.F., Jullien, L., and Lemarchand, A. (2005). Reactant concentrations from fluorescence correlation spectroscopy with tailored fluorescent probes. An example of local calibration-free pH measurement. J. Am. Chem. Soc. *127*, 15491–15505. https://doi.org/10.1021/ja053909w.
52. Haustein, E., and Schwille, P. (2007). Fluorescence correlation spectroscopy: novel variations of an established technique. Annu. Rev. Biophys. Biomol. Struct. *36*, 151–169. https://doi.org/10.1146/annurev.biophys.36.040306.132612.
53. Wang, H., Carey, L.B., Cai, Y., Wijnen, H., Futcher, B., Ying, C., Wijnen, H., and Futcher, B. (2009). Recruitment of Cln3 Cyclin to Promoters Controls Cell Cycle Entry via Histone Deacetylase and Other Targets. PLoS Biol. *7*, e1000189. https://doi.org/10.1371/journal.pbio.1000189.
54. Claude, K.L., Bureik, D., Chatzitheodoridou, D., Adarska, P., Singh, A., and Schmoller, K.M. (2021). Transcription coordinates histone amounts and genome content. Nat. Commun. *12*, 4202. https://doi.org/10.1038/s41467-021-24451-8.
55. Fu, H., Xiao, F., and Jun, S. (2023). Bacterial Replication Initiation as Precision Control by Protein Counting. PRX Life *1*, 013011. https://doi.org/10.1103/prxlife.1.013011.
56. Sachsenmaier, W., Remy, U., and Plattner-Schobel, R. (1972). Initiation of synchronous mitosis in Physarum polycephalum: A model of the control of cell division in eukariots. Exp. Cell Res. *73*, 41–48. https://doi.org/10.1016/0014-4827(72)90099-7.
57. Nash, R., Tokiwa, G., Anand, S., Erickson, K., and Futcher, A.B. (1988). The WHI1+ gene of Saccharomyces cerevisiae tethers cell division to cell size and is a cyclin homolog. EMBO J. *7*, 4335–4346.
58. Cross, F.R. (1988). DAF1, a mutant gene affecting size control, pheromone arrest, and cell cycle kinetics of Saccharomyces cerevisiae. Mol. Cell Biol. *8*, 4675–4684. https://doi.org/10.1128/MCB.8.11.4675.Updated.
59. Langmead, B., and Salzberg, S.L. (2012). Fast gapped-read alignment with Bowtie 2. Nat. Methods *9*, 357–359. https://doi.org/10.1038/nmeth.1923.
60. Digman, M.A., Dalal, R., Horwitz, A.F., and Gratton, E. (2008). Mapping the number of molecules and brightness in the laser scanning microscope. Biophys. J. *94*, 2320–2332. https://doi.org/10.1529/biophysj.107.114645.
61. Ghazal, G., Gagnon, J., Jacques, P.É., Landry, J.R., Robert, F., and Elela, S.A. (2009). Yeast RNase III Triggers Polyadenylation-Independent Transcription Termination. Mol. Cell *36*, 99–109. https://doi.org/10.1016/j.molcel.2009.07.029.
62. Tollis, S., Singh, J., Palou, R., Thattikota, Y., Ghazal, G., Coulombe-Huntington, J., Tang, X., Moore, S., Blake, D., Bonneil, E., et al. (2022). The microprotein Nrs1 rewires the G1/S transcriptional machinery during nitrogen limitation in budding yeast. PLoS Biol. *20*, e3001548. https://doi.org/10.1371/journal.pbio.3001548.
63. Bullard, J.H., Purdom, E., Hansen, K.D., and Dudoit, S. (2010). Evaluation of statistical methods for normalization and differential expression in mRNA-Seq experiments. BMC Bioinf. *11*, 94.
64. Ferrezuelo, F., Colomina, N., Futcher, B., and Aldea, M. (2010). The transcriptional network activated by Cln3 cyclin at the G1-to-S transition of the yeast cell cycle. Genome Biol. *11*, R67. https://doi.org/10.1186/gb-2010-11-6-r67.

STAR★METHODS

KEY RESOURCES TABLE

REAGENT or RESOURCE	SOURCE	IDENTIFIER
Chemicals, peptides, and recombinant proteins		
β- Estradiol	Sigma-Aldrich	CAS No.:50-28-2
1NM-PP1	Sigma-Aldrich	CAS Number:221244-14-0
Experimental models: Organisms/strains		
SWI4-GFP	This Study	MTY 5270
whi5Δ SWI4-GFP	This Study	MTY 5180
CLN3Δ SWI4-GFP	This Study	MTY 5318
mbp1Δ SWI4-GFP	This Study	MTY 5271
CDC28-as1 SWI4-GFP	This Study	MTY 5317
SWI4pr$_{Cdel}$-SWI4-GFP	This Study	MTY 5320
SWI4pr$_{Cmut}$-SWI4-GFP	This Study	MTY 5314
SWI4pr$_{C+Dmut}$-SWI4-GFP	This Study	MTY 5298
SWI4pr$_{C+D+UMut}$-SWI4-GFP	This Study	MTY 5302
Z3EVpr-SWI4 SWI4	This Study	MTY 5188
Z3EVpr-SWI4 SWI4-GFP	This Study	MTY 5189
Z3EVpr-SWI4-GFP SWI4	This Study	MTY 5190
WT diploid	This Study	MTY 5309
SWI4-GFP SWI4 diploid	This Study	MTY 5261
SWI4pr$_{Cdel}$-SWI4-GFP/SWI4 diploid	This Study	MTY 5263
Software and algorithms		
MATLAB R2018B	Mathworks	https://www.mathworks.com
SimFCS 4	Laboratory of Fluorescence Dynamics, UC Irvine	https://www.lfd.uci.edu/globals/
Bowtie 2.2.5	Langmead et al.[59]	http://bowtie.cbcb.umd.edu
Deposited data		
GEO accession number	GSE279708	https://www.ncbi.nlm.nih.gov/geo/

EXPERIMENTAL MODEL AND STUDY PARTICIPANT DETAILS

Yeast strain construction

All experiments were conducted in the derivatives of S288C strain of *Saccharomyces cerevisiae* or budding yeast. All strains used in this study and the approaches used to create them are listed in Table S5. All haploid experimental strains were generated in the BY4741 or BY4742 derivatives of the S288C background as indicated, with PCR-based homologous recombination integration of a *mGFPmut3-HIS3MX* cassette (or the corresponding *URA3*, *kan or hph* versions) at the C terminus of the *SWI4* natural locus. Tagged alleles were crossed into other BY4741/BY4742 strains as indicated. A strain producing monomeric GFP from an inducible promoter, used in molecular brightness calculations, was obtained by transforming <*pGAL1-mGFPmut3 CEN URA3*> plasmid into the BY4741 parental strain. This strain is referred to as the free GFP strain.

The β-Estradiol (BE2) inducible strains were constructed from a parental Z3EV expression strain DBy19004 (a.k.a. MTy5193; relevant genotype *ura3Δ::natMX bud9Δ::ACT1pr-Z3EV-ENO2term-URA3-Z3EVpr(P1)-GFP-GAL80term*)[34] by integration of a *mGFPmut3-HIS3MX* cassette at the C-terminal codon of the endogenous *SWI4* locus. In this strain, the Z3EV artificial transcription factor controlled by the *ACT1* promoter and *ENO2* terminator is integrated to replace the non-essential *BUD9* locus in order to express Z3EV and any gene of interest under the Z3EV-responsive promoter *Z3EVpr(P1)* (abbreviated *Z3EVpr)*, which contains binding sites for Z3EV and allows conditional expression upon β-estradiol addition to the culture. The strain referred to as *Z3EVpr-SWI4 SWI4-GFP* expressed untagged wild type *SWI4* from the Z3EV promoter the integrated *swi4::SWI4-GFPmut3* cassette (MTy5189) and was used to assess Swi4-dependent *SWI4-GFP* induction. PCR fragment-based HR was used to integrate *SWI4-hphMX* under the *Z3EV* promoter (P1) to replace GFP in strain DBy19004 and yield the *Z3EVpr-SWI4* strain MTy5188. The *mGFPmut3-kanMX* cassette was then integrated at endogenous *SWI4* locus to obtain the strain *Z3EVpr-SWI4 swi4::SWI4-GFP* (referred to as

Z3EVpr-SWI4 SWI4-GFP, MTy5189). A control strain, *Z3EVpr-SWI4-GFP SWI4* (MTy5190), was constructed in the same manner to demonstrate *SWI4-GFP* expression from the *Z3EV* promoter and measure induction at different BE2 concentrations.

SWI4 promoter deletions and mutations were introduced by CRISPR-Cas9 mediated HR with mutated repair sequences. Briefly, guide RNAs (gRNAs) were cloned into plasmid pGZ110 (kindly provided by Bruce Futcher, SUNY Stonybrook) and co-transformed with a *SWI4* promoter repair cassette (either cloned into pGZ110 or as a separate linear fragment) to introduce the mutations of interest. gRNA and repair cassette sequences are provided in Table S6. Target strains contained either wild type *SWI4* allele or a *SWI4-mGFPmut3* cassette integrated at the C-terminal codon of the endogenous locus. All mutations were confirmed by sequencing of genomic DNA. As indicated in Table S5, promoter mutations were combined with other strain genotypes by genetic crosses.

Experimental design

The objective of the study was to quantify the effects of key G1/S factors on the accumulation of the Swi4 transcription factor during cell growth in G1. To this purpose, we fused GFPmut3 (referred to as GFP for simplicity) to the Swi4 C-terminus at the endogenous *SWI4* locus, and quantified the Swi4-GFP protein levels using the scanning Number and Brightness particle counting approach as implemented in[19] and described below. Measurements were performed in isogenic strains bearing deletions/mutations of key genes or their promoters known to control the G1/S transition. None of the GFP-tagged experimental strains exhibited noticeable cell size and growth phenotype differences from their untagged counterparts.

METHOD DETAILS

Cell culture

All strains were grown in synthetic complete (SC) medium with 2.0 g/L amino acid mix (Sunrise Science) supplemented with 6.7 g/L yeast nitrogen base (Sigma-Aldrich) and 2% w/v glucose. For each sN&B experiment, a single colony of appropriate (untagged) background strain, free GFP strain and the GFP-tagged strains of interest were grown in 1 mL SC 2% glucose medium overnight. The overnight cultures were diluted 1/30 in 1 mL SC 2% glucose medium and grown to early exponential phase (4-5 h) before imaging. For synchronous time course experiments in presence of BE2, early G1 cells obtained by centrifugal elutriation were induced with 5 nM or 0 nM BE2 in SC 2% glucose medium for 15 min at 30°C, and added to SC 2% glucose agarose pads containing 5 nM or 0 nM BE2 prior to imaging. The strain expressing the analog sensitive allele of the Cdc28 kinase was induced with 10 μM of the ATP analog drug, 1- (tert-butyl)-3-(naphthalene-1-lmethyl)-1H-pyrazolo [3,4-d] pyrimidin-4-amine, referred to as 1-NM-PP1, directly on agarose pads. Cells were grown on these pads for 20 min prior to imaging. For GFP induction of the *pGAL1-GFPmut3* strain used for GFP brightness calibration (free GFP strain), after overnight growth to saturation in SC glucose medium, the culture was washed, diluted 1/30 and grown in SC 2% raffinose medium for 3-4 h, followed by the addition of 0.1% galactose to the culture for 1 h. The induced culture was then washed twice with SC 2% glucose medium and grown in SC 2% glucose medium for 3-4 h before imaging under similar growth and culture conditions as the control and protein fusion strains.

Preparation of agarose pads

Before each sN&B experiment, 200 μL from a 1 mL culture grown to early exponential phase (OD600 of 0.16-0.18, cell density 1-2 x 10^6 cells/mL) was pelleted in a microfuge at 1300 rpm for 30 seconds and 195 μL of the supernatant was discarded. Cells were immediately re-suspended in the remaining 5 μL medium, and 3.5 μL of the suspension was mounted onto a 2% glucose agarose pad (62μL) as previously described.[19] The agarose pad containing mounted cells was sealed with a ConA (Sigma, 2 mg/mL)-coated coverslip for immobilization of cells during imaging. The sealed pads were clamped in an Attofluor chamber (Molecular Probes) and clusters of monolayer cells were imaged for no longer than 2 h.

Elutriation of BE2-dependent strains

Centrifugal elutriation was used to isolate synchronous G1 cells for the time-course imaging of WT *SWI4* (MTy 5270) and BE2-inducible *SWI4* strain (MTy 5189). Cells were cultured in 1.2 L of SC + 2% glucose overnight to early exponential growth phase ($0D_{600}$=0.14 measured using a Tecan Infinite M1000 Pro Plate Reader), and centrifuged in a Sorvall SLC-6000 rotor at 1100 rpm for 10 min at 4°C. Cells were re-suspended in 50mL of the supernatant, lightly sonicated (30 s, 1 s intervals at power level 1). The elutriator was pre-filled with fresh medium at a flow rate of 30 mL/min for 5 min at 1500 rpm. Then the flow rate was decreased to 8 mL/min, medium was switched to the medium in which the cells to be elutriated were grown and cells were loaded into the elutriator (Beckman JE-5.0 rotor) at 8 mL/min at 1500 rpm and then elutriated at 12 mL/min in 50 mL fractions. 200 μL of an elutriated G1 fraction was pelleted in a microfuge at 1300 RPM for 30 seconds and 195 μL of the supernatant was discarded. Cells were immediately re-suspended in the remaining 5 μL medium. Finally, 3.5 μL of the suspension was mounted onto a 2% glucose agarose pad (62μL) as previously described.[19]

Scanning number and brightness (sN&B) imaging

For accurate quantitative measurement of absolute concentrations of Swi4-GFP, we used an image based particle-counting fluctuation microscopy technique called sN&B (Methods S1).[60] The sN&B acquisitions were performed in an ISS Alba fast scanning mirror fluctuation microscope (ISS, Champaign, IL) equipped with 2-photon laser excitation (Mai Tai Ti: Sapphire, Newport-SpectraPhysics,

Mountain View, CA) at an excitation wavelength of 1000 nm. Emission from GFP was obtained using a 530 +/- 50 nm band-pass filter. Acquisition for each strain was done in multiple Fields of View (FOVs) with the FOV size of 256x256 pixels covering 20x20 μm. Each FOV was scanned with 50 raster scans at a 40 μs pixel dwell-time at an excitation power of 30-35 mW. Further, each FOV was imaged in 3 z-positions separated by 500 nm.

Steady-state and time course imaging of BE2-dependent strains

In steady-state BE2 experiments, the WT *SWI4-GFP* strain (MTy 5270) and the experimental and control *Z3EV SWI4-GFP* strains, MTy5189 and MTy5190, respectively, were imaged as for all other strains except that in addition cells were incubated for 30 min in SC medium containing 0-5 nM of BE2 after reaching the early exponential phase of growth. The BE2-induced cultures were centrifuged, the supernatant removed, and induced cells were grown in 1mL SC 2% glucose media for 1 h before mounting on agarose pads for imaging.

In the BE2 time courses, early G1 cells of WT *SWI4-GFP* (MTy5270) and the BE2 strains (MTy5189 and MTy5190) obtained through centrifugal elutriation were treated with 5 nM BE2 for 15 minutes and mounted onto a 2% glucose agarose pad containing BE2 as described above. The cells were imaged as above at 31% power or about 30mW power. To avoid photobleaching, a new FOV was imaged at every time point for 10 scans at 40 μs pixel dwell time at 3 z-positions separated by 500 nm.

Coulter counter cell sizing and growth curve

The population size distributions of all strains were determined using a Beckman Coulter Counter Z2 particle sizer calibrated to a default aperture size of 50 μm and 31.02 diameter calibration constant, with the upper and lower size threshold for particles set to 7.256 and 2.255 μm, respectively. Overnight cultures from a single colony were diluted 1:30 in 1 mL SC 2% glucose medium and grown to early exponential phase (4-5 h). 200 μL of culture was added to 10 mL of Beckman Isoton II diluent solution and sonicated lightly for 30 seconds before size acquisition. The number of cells per binned cell size window were divided by the total particle count to yield the fraction of cells in each size bin, referred to as "cell size distribution". For assessing the growth rate of different strains, cells were grown and diluted as above in SC 2% glucose medium and measured every hour in a Grenier 96-well flat well transparent plate at 600 nm (OD600). The doubling time was assessed from the slope of the linear part of the growth curve, that corresponds to log phase.

RNA-seq

The *Z3EVpr-SWI4 SWI4* (MTy5188) cells were grown as described above for sN&B experiments and induced for 1 h with either 5 nM of BE2 (in ethanol solvent) or with ethanol as a negative control. Total RNA was prepared as described in[61] both before (pre-induction sample) and after induction. Briefly, cells were disrupted using glass beads, and their aqueous content was extracted using phenol/chloroform. Nucleic acids were then precipitated using ethanol and genomic DNA was removed using DNase treatment (Qiagen). RNA was quantified using Qubit (Thermo Scientific) and assessed for quality with a 2100 Bioanalyzer (Agilent Technologies). Poly-A selected transcriptome libraries were generated using the Kapa RNA HyperPrep (Roche). Sequencing was performed on an Illumina NextSeq 500 system at the IRIC genomic platform. Experiments were performed in duplicate.

QUANTIFICATION AND STATISTICAL ANALYSIS

Scanning number and brightness image analysis

Methodology for sN&B analysis has been described previously,[19] but is briefly summarized here and in Methods S1 for ease of reference. For absolute quantification of fluorescent proteins using sN&B, we used probabilistic auto-fluorescent background subtraction, based on comparing the distribution of background intensities from hundreds of millions of pixels of images from cells that do not express GFP fusions in order to generate a probabilistic calculation of the auto-fluorescent background intensity contribution at every pixel in the FOV from cells expressing specific GFP fusions. Two calibration parameters were performed for obtaining the absolute concentrations of GFP-tagged proteins. First, the effective volume of the microscope, V_{PSF}, defined by laser alignment, was obtained for each experiment by sN&B using a solution of 46 or 28 nM fluorescein in Tris buffer (pH 8.0) and 40% glycerol. Second, an *in cellulo* sN&B calibration of the molecular brightness of free monomeric GFP, e_{GFP}, was performed using cells expressing monomeric GFP from a <*pGAL1-mGFPmut3 CEN URA3*> plasmid[19] to compute the concentrations of the GFP fusion proteins. For the *SWI4-GFP* strains examined, the absolute concentration of nuclear Swi4-GFP in each cell was calculated from the average intensity of all nuclear pixels after background subtraction, $\langle F \rangle_{nuc}$, as:

$$[Swi4]_{nuc}(M) = \langle F \rangle_{nuc} / e_{GFP} V_{PSF} N_A$$

where N_A is the Avogadro number. Nuclear volume for individual cells was calculated as 1/7 of the total cell size[28] derived from whole cell masking and assuming a sphere. We note that nuclear volume scale slightly sub-linearly with respect to cell size,[22] but this small effect did not significantly affect results drawn for Swi4.

All sN&B acquisitions were analyzed using custom 2015 MATLAB scripts (Sylvain Tollis, University of Montreal with edits from Steven Notley and Catherine Royer, RPI), which has previously been used to determine absolute concentration of fluorescent proteins in

live cells.[19,62] This semi-automated analysis allowed the computation of absolute protein concentrations in the best Z-position for selected regions of interest i.e., the nucleus of pre-Start cells.

Intensity analysis

All analysis of fluorescence intensity of Z3EV strains were performed in the analysis software SimFCS (Enrico Gratton, Laboratory of Fluorescence Dynamics, UC Irvine). Fluorescence intensity from 5 FOVs at each concentration were averaged and plotted in Figure 4. All fluorescence intensity images used SimFCS at 0-14 intensity units as the scale. Error bars represent the standard error of the mean from the value of average nuclear Swi4 concentration of all the cells between two replicates.

RNA-seq analysis

RNA-sequencing data analysis was performed as detailed in.[62] Briefly, raw reads were aligned to all Ensembl yeast transcripts using Bowtie 2.2.5[59] with default parameters and counts defined as alignments with an edit distance smaller than 5. Dubious ORFs as annotated in the Saccharomyces Genome Database (yeastgenome.org) were excluded. Only genes with at least 500 reads in one sample were further analyzed. Gene expression levels were expressed as log2 read counts, normalized to the upper-quartile gene expression level for each sample separately.[63] For each of the two replicates, the expression after 1 hour induction was normalized separately to the expression in the pre-induction sample and in the control ethanol-treated sample of the same replicate, yielding four-fold-analog change values for each gene. Then, the smallest of these log2 fold-changes (in absolute value) was used to generate the final differential expression profile represented on Figure 6. Hence, a gene had to be upregulated (or downregulated) with respect to both the pre-induction *and* the ethanol-treated control sample across both replicates to yield a positive (or negative) score. The former control reduced sample-to-sample variation while the second control eliminated BE2-independent but time-dependent gene expression variation in the cell population. Genes for which any of the four normalizations yielded log2 fold changes of different signs were assigned a score of 0. Among the most up- and down-regulated genes, direct SBF and/or MBF targets were identified based on the G1/S regulon gene list defined by Ferrezuelo et al.[64] At each ranking position n, the enrichment of SBF targets (for upregulated genes) or MBF targets (for downregulated genes) within the n^{th} top differentially regulated genes as compared to random expectations was computed, and the significance of the enrichment level was calculated using Fisher's exact test.